Eur Radiol (2002) 12:1022–1044
DOI 10.1007/s00330-002-1342-1

New frontiers in CT imaging of airway disease

Philippe A. Grenier
Catherine Beigelman-Aubry
Catalin Fétita
Françoise Prêteux
Michel W. Brauner
Stéphane Lenoir

Received: 10 January 2001
Accepted: 16 January 2001
Published online: 15 March 2002

P.A. Grenier (✉) · C. Beigelman-Aubry
Department of Radiology,
Assistance Publique–Hôpitaux de Paris,
Pitié-Salpêtrière Hospital,
University Pierre et Marie Curie,
47–83, boulevard de l'Hôpital,
75651 Paris, France
e-mail:
philippe.grenier@psl.ap-hop-paris.fr
Tel.: +33-1-42178225
Fax: +33-1-42178224

C. Fétita · F. Prêteux
Institut National des Télécommunications,
Department ARTEMIS, Evry, France

M.W. Brauner
Avicenne Hospital, UFR SMBH Paris XIII,
Bobigny, France

S. Lenoir
Institut Mutualiste Montsouris, Paris,
France

Abstract Combining helical volumetric CT acquisition and thin-slice thickness during breath hold provides an accurate assessment of both focal and diffuse airway diseases. With multiple detector rows, compared with single-slice helical CT, multislice CT can cover a greater volume, during a simple breath hold, and with better longitudinal and in-plane spatial resolution and improved temporal resolution. The result in data set allows the generation of superior multiplanar and 3D images of the airways, including those obtained from techniques developed specifically for airway imaging, such as virtual bronchography and virtual bronchoscopy. Complementary CT evaluation at suspended or continuous full expiration is mandatory to detect air trapping that is a key finding for depicting an obstruction on the small airways. Indications for CT evaluation of the airways include: (a) detection of endobronchial lesions in patients with an unexplained hemoptysis; (b) evaluation of extent of tracheobronchial stenosis for planning treatment and follow-up; (c) detection of congenital airway anomalies revealed by hemoptysis or recurrent infection; (d) detection of postinfectious or postoperative airway fistula or dehiscence; and (e) diagnosis and assessment of extent of bronchiectasis and small airway disease. Improvement in image analysis technique and the use of spirometrically control of lung volume acquisition have made possible accurate and reproducible quantitative assessment of airway wall and lumen areas and lung density. This contributes to better insights in physiopathology of obstructive lung disease, particularly in chronic obstructive pulmonary disease and asthma.

Keywords Chronic obstructive pulmonary disease · Airways · Helical CT · 3D images

Introduction

Helical CT is the recommended imaging technique for assessing the airways. Owing to its capability for continuous volume acquisition during a single breath hold, helical CT provides a super tool to visualize even minor intra- and extraluminal pathology in the trachea and proximal bronchi. Bronchial tumors and inflammatory stenoses can be reliably depicted. Postprocessing analysis techniques including multiplanar reformation, 3D surface display, volume-rendering technique and virtual bronchoscopy are valuable in the evaluation of extent of stenosis for planning treatment and follow-up. Thin-section (high-resolution) CT at inspiration and expiration has gained wide acceptance of the imaging modality of choice in the evaluation of distal airways. It is particularly appreciated for the diagnosis and assessment of extent of bronchiectasis and small airway disease. To date, by combining both helical volumetric acquisition and thin slice thickness over the entire lungs during a single breath hold, multislice CT offers the advantage of providing an accurate assessment of focal or diffuse, proxi-

mal or distal airway disease. Continued improvement in quantitative image-analysis techniques and the use of spirometrical control of the lung volume at acquisition make it possible to more easily assess airways lumen and wall areas and lung density. This quantitative assessment of the airways will lead to the increasing use of CT as a research tool for better insights in physiopathology of obstructive lung disease, particularly in chronic obstructive pulmonary disease (COPD) and asthma, with an ultimate benefit in clinical practice

Acquisition parameters and image processing

Using state-of-the-art single-detector helical CT scanners with subsecond rotation time (0.5–0.8 s), an acceptable compromise is reached using 2- or 3-mm collimation, a pitch value ranging from 1.5 to 2, 30–50% overlap index in reconstruction, and a low spatial resolution algorithm [1, 2, 3]. Introduction of the multidetector-row technology allows now the performance of fast acquisitions of around 20 s for the entire thorax while using 1-mm slice thickness. Because slice thickness has the greatest impact on the quality of 3D reconstructions [2], the overall quality of 3D simulations is increased [1, 4].

Because of the great natural contrast between the airways and their environment, low kilovoltage (100–120 kV) and milliamperage (100–150 mAs) may be used [1]. Visualization of the overlapped thin axial images sequentially in a cine mode allows the bronchial divisions to be followed from the segmental origin to the distal bronchial lumens down to the smallest bronchi which can be identified on thin section images. This viewing technique helps indicate the segmental and subsegmental distribution of any airway lesion and may serve as a roadmap for the endoscopist. Moving up and down through the volume at the monitor has become an alternative to film-based review. Image processing includes multiplanar reformations and techniques that produce 3D images, such as minimum intensity projection, 3D surface-shaded display and volume rendering [1]. In all cases the first procedure is the acquisition of a primary volume data set from a helical CT consisting of overlapping transaxial images, which provide the highest morphologic detail [3]. The z-axis resolution is directly related to the effective slice thickness. The smaller the effective slice thickness, the more precise are 2D reformats or 3D reconstructions [3]. The optimal effective slice thickness is therefore of 1.5 mm or less. It is critical to point out that any technique used to view the CT data through any plane other than the transverse plane or projection other than the craniocaudal projection results in an image with anisotropic pixels. The in-plane resolution is defined y the reconstruction kernel and field of view, whereas the through-plane or z-axis resolution is defined by the collimator width, pitch, and interpolation algorithm. Therefore, as the angle of the reformation plane increases relative to the plane of acquisition, spatial resolution decreases. The highest resolution views for evaluating helical CT scans, regardless of application, are the unedited transverse CT sections. They should always be carefully reviewed at appropriate window and level settings regardless of additional rendering techniques employed [5].

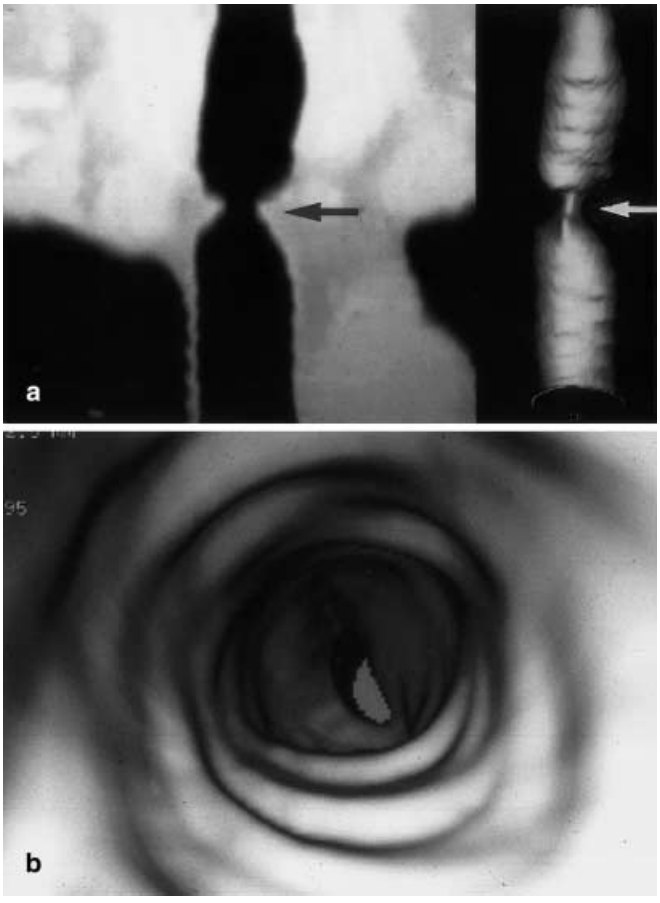

Fig. 1a, b Tracheal stenosis occurred as a complication of tracheostomy. **a** Coronal oblique image of the trachea reformatted after helical CT acquisition showing the exact location and degree of the stenosis (*left*). The 3D surface shadowing display image (*right*) demonstrates the asymmetric aspect of the stenosis. **b** Descending virtual endoscopy view assesses the internal morphology of the stenosis

Multiplanar reformations

Multiplanar reformations allow to obviate the underestimation of the limits of the craniocaudal extent of a vertically oriented disease such as tracheobronchial stenosis (Fig. 1). They are of particular value for better detection and evaluation of mild focal stenosis [6]. They are also well appreciated in the assessment of congenital abnor-

Fig. 2 Minimal intensity projection in the coronal direction of the proximal airways after multislice CT acquisition with thin slice thickness. A linear hypoattenuation area lying perpendicular to the long axis of the trachea (*black arrow*) corresponds to the presence of air in the esophagus. This is an artifact simulating a tracheal fistula

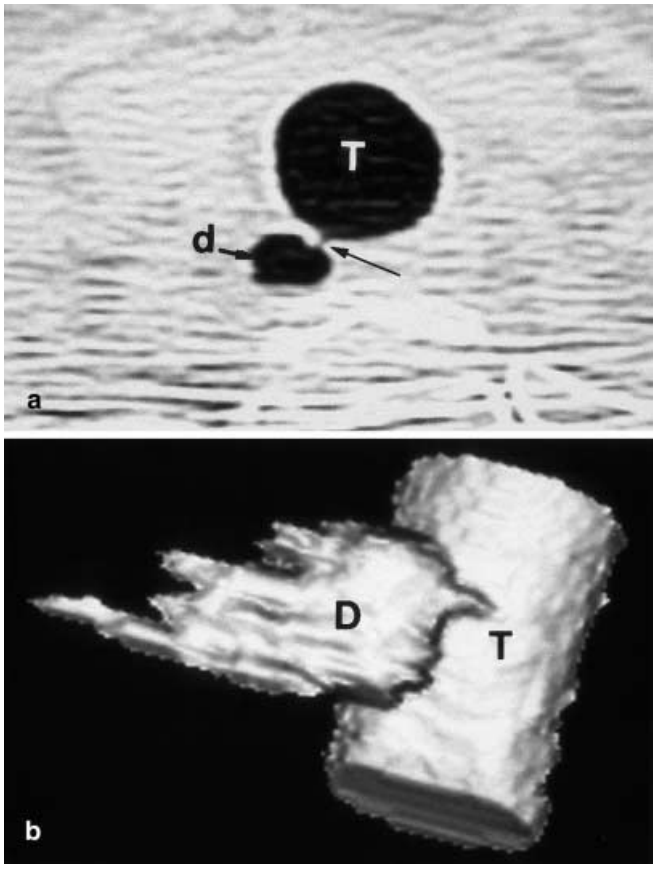

Fig. 3a, b Tracheal diverticula. **a** Axial thin slice of the trachea showing a rounded air collection (*d*) located right and posterolateral to the trachea (*T*). That air collection is connected to the tracheal lumen by a tiny tracheal wall dehiscence (*arrow*). At surgery, this lesion was resected and corresponded to a congenital diverticula of the trachea. **b** The 3D surface-shaded display image shows the relationships between the diverticula (*D*) and the tracheal lumen (*T*) on a right lateral view

malities of the tracheobronchial tree and in the diagnosis of bronchial dehiscence following lung transplantation or surgery [7]. Whereas the thickness of the displayed planar image is 0.6–0.8 mm, depending on the dimension of the field of view, multiplanar volume reconstruction (MPVR) consists of a slab with a thickness of several pixels and of a less noisy reformation [8]. Underestimation of a stenosis, however, may occur if the reformation plane is not adequately chosen. This can be avoided by a simultaneous reading of the native cross-sectional images and a selection of reformation plane from the 3D reconstructed image of the airways [7].

Minimum intensity projection imaging

Minimum intensity projection (MIP) imaging is a simple form of volume rendering that is able to project the tracheobronchial air column into a viewing plane. It is usually applied to a selected volume of the thorax containing the airways under evaluation (sliding thin slab or MPVR-MIP technique). Pixels encode the minimum voxel value encountered by each ray. Airways are visualized because air contained within the tracheobronchial tree is lower in attenuation than surrounding pulmonary parenchyma, with a small density difference between pulmonary parenchyma and airways between 50 and 150 HU [5]. Minimum intensity projection, however, is rarely used in the evaluation of the airways because numerous drawbacks have limited its indications in assessing airway disease. The size of asymmetrical stenoses may be artificially decreased [8]. The technique is very vulnerable to varying width of volume of interest and to partial-volume effects [3]. Even minor partial-volume averaging leads to underestimation of the airway caliber. This effect grows with increasing effective slice thickness, decreasing bronchial diameter, and horizontal course of a bronchus [3]. Sometimes, high-grade stenoses can be imaged as pseudo-occlusions. The intraluminal growth of eccentric tumors is generally underestimated and may even be completely missed. Intraluminal structures of higher density (e.g., stents) are not displayed. Other air-containing structures, such as esophagus, may simulate tracheal fistulas if careful analysis of all angles of view is not performed (Fig. 2).

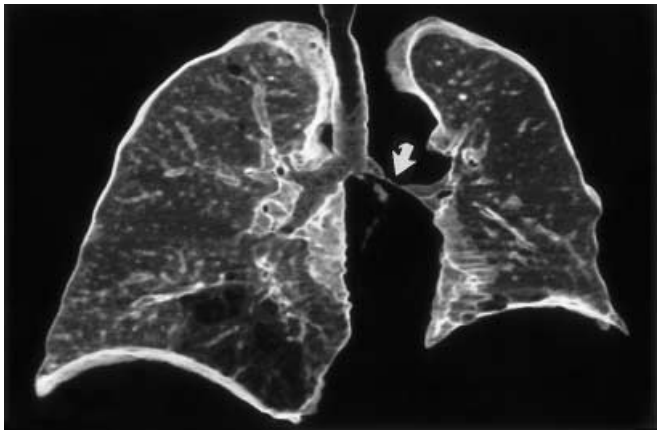

Fig. 4 Volume rendering of the airways and lung parenchyma after multislice CT acquisition in a patient with Wegener's granulomatosis. A narrow and regular stenosis is visualized on the left main bronchus (*arrow*). Note the presence of emphysema in the right lower lobe

3D surface rendering technique with shaded display

The surface of the volume of air contained in the airways is isolated from the initial volume data by thresholding segmentation [7, 8, 9]. The depth impression is optimally rendered by shading the surface obtained from depth encoding. The technique allows for a better understanding of the longitudinal extent of airway stenoses than axial CT images (Fig. 1). The 3D images offer an overview of the pathology, particularly appreciated in complex airway anatomy (i.e., bronchial distortion following surgery). It also may identify extraluminal air (i.e., tracheobronchial diverticuli, fistulae, and air leaks) (Fig. 3). The major limits of this technique are related to thresholding range. The degree of airway stenosis rendered by a 3D surface-rendering technique will increase with the threshold of segmentation, and vice versa. The result of reconstruction is also sensitive to partial-volume artifacts, stair-step artifacts, and motion-related artifacts [7]. In addition, voxels fractionally composed of the tissue and air are not integrated in the final image [8].

Virtual bronchography

Volume-rendering technique applied at the level of central airways allows reconstruction of 3D images of the airways visualized in semi-transparent mode similar to conventional bronchograms (Figs. 4, 5). This leads to a new functionality called virtual bronchography. To segment the lumen–wall interface of the airways, Rémy-

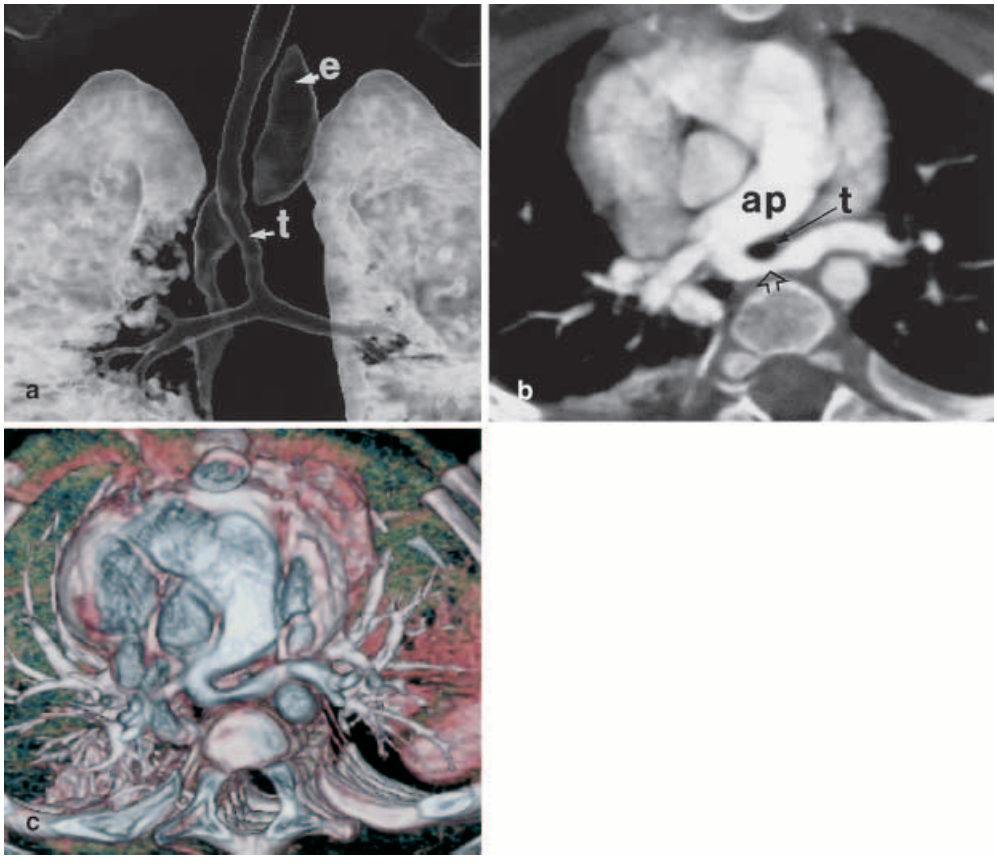

Fig. 5a–c Left retrotracheal pulmonary artery in a 4-year-old boy. **a** Volume rendering of the airways and lung parenchyma after multislice CT acquisition in the coronal view showing the left displacement and abnormal course of the distal part of the trachea, carina, and right main bronchus. The lumen of the distal part of the trachea (*t*) is reduced in caliber. Air in the esophagus is also depicted (*e*). **b** Axial CT scan with bolus injection of contrast material showing the abnormal position and course of the main pulmonary artery. The left pulmonary artery is in a right position to the trachea (*t*) then runs to the left (*arrow*) behind the trachea (*t*). **c** Volume rendering of the vessels in the axial view confirms the relationships between the left pulmonary artery, tracheal lumen, and spine

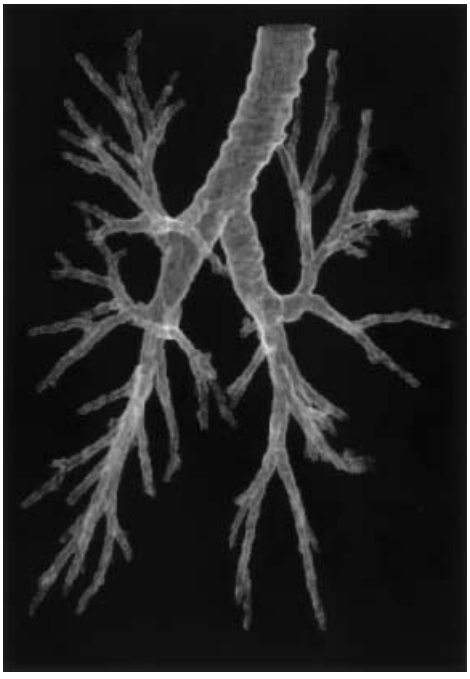

Fig. 6 Virtual bronchography (volume rendering of the segmented airways after multislice CT acquisition, 1-mm slice thickness, and 0.6-mm overlap in reconstruction) in the oblique view (left posterior oblique). Normal appearance of the airways in a mild intermittent asthmatic patient

Jardin et al. used a continuous rim of peripheral voxels (70% of opacity value) and the volume-rendering algorithm [10]. They demonstrated in a series of 74 patients known or suspected of airway disease, that virtual bronchography added diagnostic or morphologic information in 31% of patients [11]. Virtual bronchography was of particular interest in diagnosing mild changes in airway caliber and understanding complex tracheobronchial abnormalities. With Fetita et al., we have developed a fully automatic method for 3D bronchial tree reconstruction [12]. It is based on bronchial lumen detection within the thoracic volume data set obtained from a helical CT acquisition with thin slice thickness during breath hold. The reconstruction approach relies on a region-growing technique conditional to a Markovian model. It involves different potential functions which exploit the structural and topologic features of the airways, thus making it possible to achieve the reconstruction of the bronchial tree up to the seventh-order division (Fig. 6). The initial kernel which originates the growth is automatically located inside each connected component of the bronchial lumen (even in the regions where the lumen presents with severe stenosis or contains mucoid impaction), to avoid inclusion of small non-bronchial air areas present in the pulmonary parenchyma. The growth initiation procedure exploits a new concept in mathematical morphology called topographical constrained connection cost which is able to extract from a gray-level volume the local valleys (airways) whose spatial extent is locally comprised in a given interval chosen between the noise and the diameter of the tracheal lumen. In order to increase the investigation capabilities of the reconstructed bronchial tree, two complementary tools have been developed:

1. Automatic delimitation and indexation of anatomical segments making possible local and reproducible analysis at a given level of the bronchial tree
2 An automatic extraction of the central axis of the bronchial tree which simplifies the interactivity during the navigation within virtual bronchography or virtual endoscopy modes

These tools can also be used for quantitative assessment of the wall and lumens of the airways on cross-sectional images of the bronchi reconstructed perpendicular to their central axis.

Virtual bronchoscopy

Virtual bronchoscopy provides an internal rendering of the tracheobronchial walls and lumen. Owing to a perspective-rendering algorithm, this simulates an endoscopist's view of the internal surface of the airways. The observer may interactively move through the airways. This technique may be obtained from both 3D surface rendering and volume-rendering techniques (Figs. 7, 8). Volume-rendering technique is less sensitive to partial-volume effects than surface rendering. Powerful computers permit real-time rendering (15–25 images/s) making flying within the airways in a virtual manner possible. Virtual endoscopy is applicable to the central airways including the subsegmental bronchi. The technique allows accurate reproduction of major endoluminal abnormalities with an excellent correlation with fiberoptic bronchoscopy results regarding the location, severity, and shape of airway narrowing [13]. Virtual endoscopy is also able to visualize the bronchial tree beyond an obstructive lesion and thus to perform a retroscopy when looking back toward the distal part of the stenosis. In addition, volume-rendering technique permits visualization of peribronchial structures through bronchial walls. This helps plan transbronchial, transtracheal, or transcarinal needle punctures [14]. Despite these appreciable abilities, virtual endoscopy remains very sensitive to the partial-volume averaging effect and motion artifacts. Discontinuities in the walls of airways can be artifactually created and structures typically appear irregular due to the polygonal modeling applied to the surfaces [4, 5]. In addition, we must never forget that virtual endoscopy is unable to identify the causes of bronchial obstruction [1]. Mild stenosis, submucosal infiltration, and superficial spreading tumors are not identified [8]. In all cases axial CT images remain the major modality for an accurate assessment of the airways.

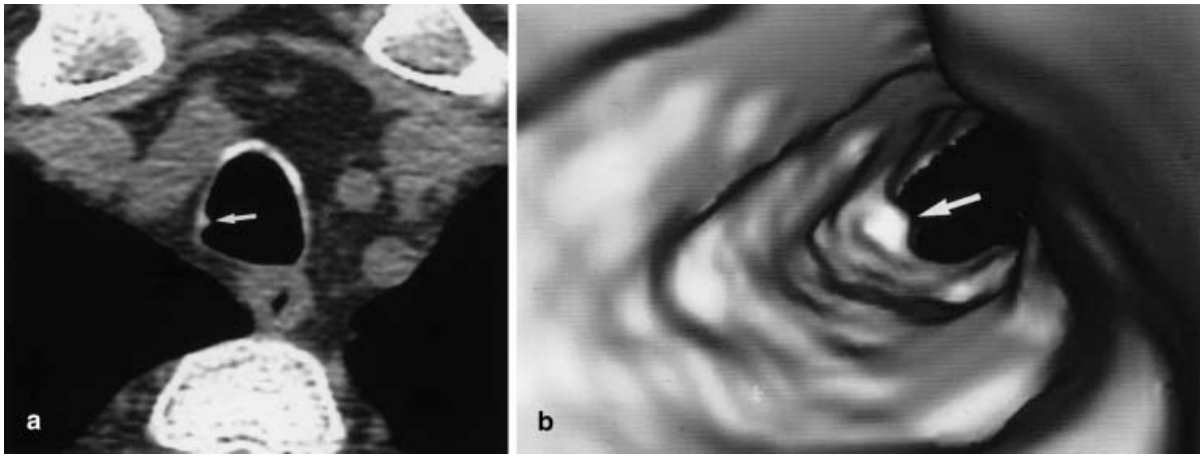

Fig. 7a, b Virtual bronchoscopy. Patient with Wegener's granulomatosis. **a** Thin-slice axial image showing a small nodular lesion on the internal margin of the tracheal lumen suggesting a granulomatous lesion. **b** Virtual endoscopy in the same patient after multislice CT acquisition showing the same lesion (*arrow*) and a multiple nodular appearance of the internal wall of the trachea completely concordant with the appearance at the real bronchoscopy

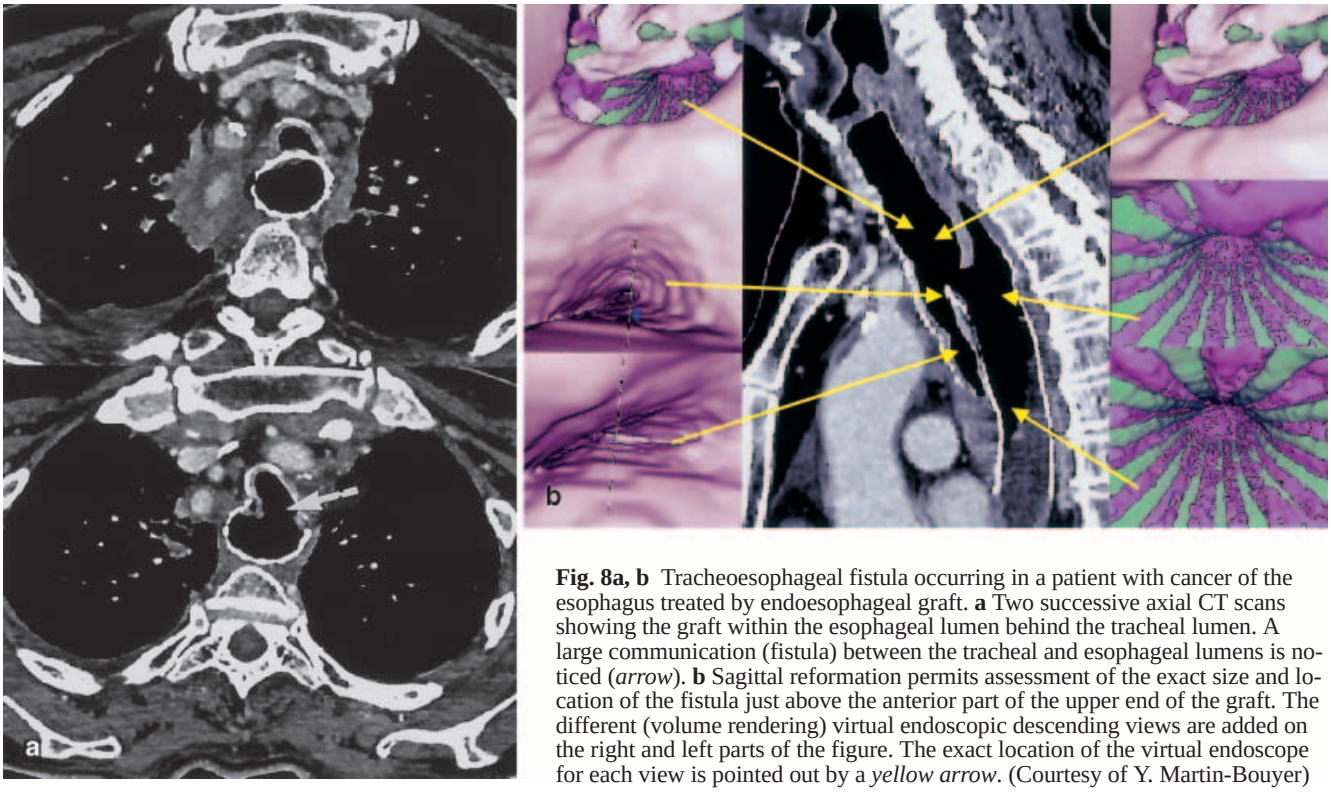

Fig. 8a, b Tracheoesophageal fistula occurring in a patient with cancer of the esophagus treated by endoesophageal graft. **a** Two successive axial CT scans showing the graft within the esophageal lumen behind the tracheal lumen. A large communication (fistula) between the tracheal and esophageal lumens is noticed (*arrow*). **b** Sagittal reformation permits assessment of the exact size and location of the fistula just above the anterior part of the upper end of the graft. The different (volume rendering) virtual endoscopic descending views are added on the right and left parts of the figure. The exact location of the virtual endoscope for each view is pointed out by a *yellow arrow*. (Courtesy of Y. Martin-Bouyer)

Quantitative CT assessment of airways

Airway lumen and airway wall areas may be quantitatively assessed on CT images by using specific techniques that must be reproducible as well as accurate in order to compare the airways pre- and postintervention (bronchoprovocation, bronchodilatation, therapeutic response) and to carry out longitudinal studies of airway remodeling. Airway lumen and wall areas measured on axial images depend on the lung volume, and angle between the airway central axis and the plane of section. Volumetric acquisition at controlled lung volume is re-

Fig. 9 Spirometrically triggered CT. View of a patient breathing through a small spirometer while positioned on the CT scan table

quired in order to precisely match the airways of an individual on repeated studies. The control of lung volume at CT is obtained by spirometrically triggering. During exhalation the spirometer and associated microcomputer measure the volume of gas expired and trigger CT after the specific volume is reached (Fig. 9). When the trigger signal is generated, air flow is inhibited by closure of mechanical occlusion device attached to the spirometer and scanning starts.

Measurements of airway lumen and wall area have to be restricted to airways that appear to have been cut in cross section based on the apparent roundness of the airway lumen. Measuring airway lumen and airway walls when they are not perpendicular to the scanning plane may lead to significant errors, the magnitude of which will depend on how acutely the airways are angled, the collimation, and the field of view. The larger the angle and field of view and the thicker the collimation, the greater the overestimation airway wall area. Most of the airways examined in axial CT slices are also more likely to be running obliquely to the plane of the section, rather than perpendicularly owing to the anatomy of the lung. With the new generation of multislice CT scanner, it becomes possible to acquire a volume of lung with 0.6- to 0.75-mm slice thickness or less and to reconstruct axial images every 0.6 mm or less by interpolation. In such a maneuver, the CT voxels may be converted into cubic dimension (isotropic voxels). Then the segmentation of bronchial lumens and reconstruction of the airways in 3D allow determination of the central axis of the airways and reconstruction of the airway cross section in a plane perpendicular to this axis (Fig. 10). This analysis technique overcomes the major limitation to the use of HRCT in quantitative analysis, which is that accurate or true airway lumen and airway wall area can only be measured from airways which are oriented approximately perpendicular to the plane of scanning.

Different image analysis techniques have been developed to make measurements of airways dimension on CT scans. McNamara et al. [15] modified a method developed by Webb et al. [16] based on visual analysis of photographed images. They found that it was crucial to use a window level of –450 HU. Amirav et al. [17] developed a computerized algorithm for measuring airway lumen area, based on an edge detection method using the full width at half maximum principle, which has advantages of less subjectivity and greater speed than the method of McNamara et al. [15]. With Prêteux et al., we developed an automatic method for segmentation and calculation of airway lumen areas based on mathematical morphology theory, marking techniques derived from the concept of connection cost, and conditional watershed segmentation [18]. Wood et al developed an algorithm to measure airway lumens and the airway angle of orientation using a 3D reconstruction of the lung [19]. This technique allowed cross-sectional images of the airways to be generated irrespective of airway of orientation. King et al. more recently developed an automatic CT image analysis algorithm to measure not only the airway lumen areas but also the wall areas and angle of orientation of airways [20]. Perot et al. [21] had a different approach with results similar to those of King et al. [20]. These results proved to be more accurate than those obtained with manual methods. All these analysis algorithms have been validated using data from phantom studies [15, 17, 18, 19, 20] and excised animal lungs [20, 21], or by developing a realistic modeling of airways and pulmonary arteries included in CT scans of animal lungs obtained in vivo [18]. Their accuracy in measuring the airways lumen [15, 17, 18, 20] and wall [20, 21] areas was very good only for bronchi measuring at least 2 mm in diameter. These techniques have been used to quantify the magnitude and distribution of airway narrowing in excised lung animals and in animal lungs in vivo as well as in normal and asthmatic subjects [15, 17, 22, 23, 24]. Although they have been used almost exclusively for research purposes, they will, with continued refinements, eventually be of benefit in the clinical practice of radiology [25].

Expiratory CT

Expiratory air trapping is a key finding for depicting an obstruction on the small airways [26]. Normally, with

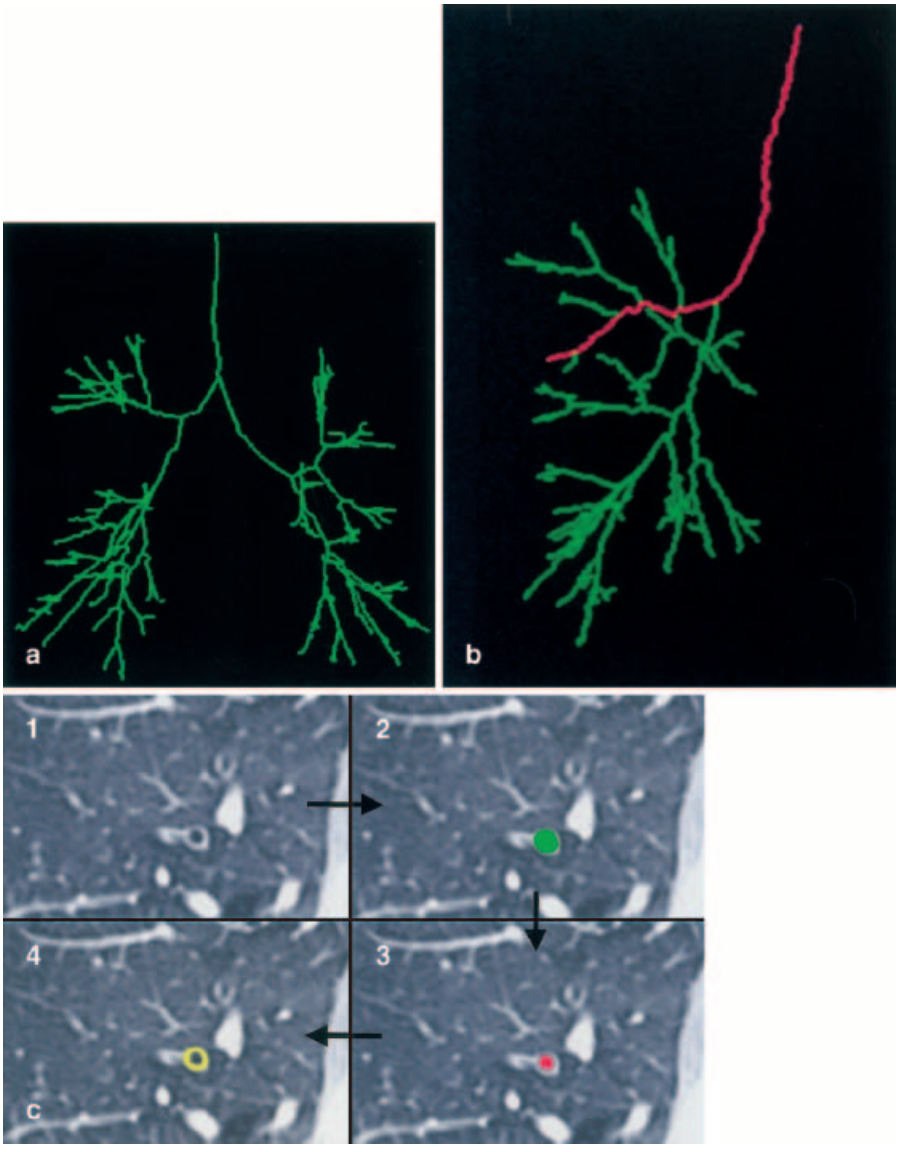

Fig. 10a–c Quantitative assessment of the airways. **a** A 3D representation of the central axis of the bronchial tree obtained from virtual bronchography. **b** Navigation (*red*) through the central axis of the bronchial tree permits selection of a specific point for quantitative assessment of the airway. **c** A 2D reformatted image of a selected bronchus in a plane perpendicular to the bronchial central axis (*1*); *2* illustrates the result of the segmentation of the external contour of the bronchial cross section and calculation of the airway area (*green*); *3* shows the results of the segmentation of the internal contour and calculation of the airway lumen (*red*), and by subtracting both, airway wall area (*yellow*) can be segmented and calculated (*4*)

expiration, lung attenuation increases due to a reduction in gas volume within the lung, whereas the cross section area surface of the lung decreases. Usually, dependent lung regions show a greater increase in lung density during expiration than do non-dependent lung regions. As a result, the anteroposterior attenuation gradients normally seen on inspiratory scans are significantly greater on expiratory scans. The anteroposterior lung attenuation gradient can have a lobar component on expiratory scan. Often the posterior aspect of the upper lobe, anterior to the major fissure, appears denser than the anterior aspect of the lower lobe, behind the major fissure. Some focal areas of low attenuation may also be seen near the tip of the lingula. Air trapping may be depicted in some individual lobules in dependent regions of the lungs. The phenomenon of greater density and physiologic air trapping in some individual lobules in dependent regions of the lung may be present irrespectively to the patient's position. All these physiologic low attenuation areas involved less than 25% of the cross-sectional area of one lung at one scan level.

Air trapping may be depicted on expiratory CT scans in approximately of 50% of asymptomatic subjects. The frequency of air trapping increases with age and its severity increases with age and smoking [27]. In smokers, the extent of air trapping is related to the smoking history independently of current smoking habits [28]. Air trapping can be considered abnormal when it affects a volume of lung equal to or greater than a pulmonary segment and are not limited to the superior segment of the lower lobe (Fig. 11). Abnormal air trapping is the finding of small airway disease, but it may also be seen beyond

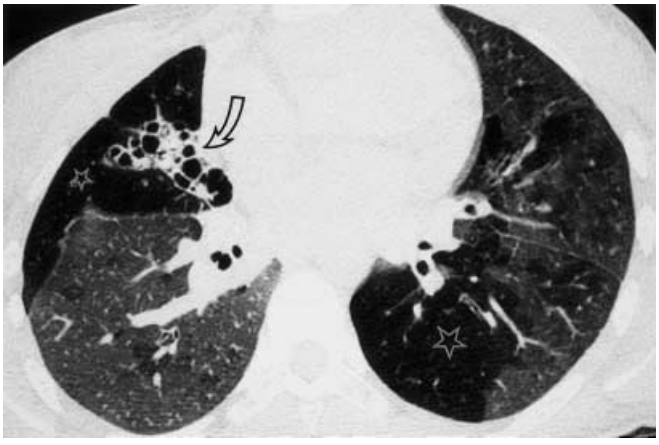

Fig. 11 Abnormal expiratory air trapping in a patient with postinfectious constrictive bronchiolitis and bronchiectasis. Postexpiratory thin section scan at the level of the right inferior pulmonary vein shows a decrease in lung attenuation and perfusion areas within the right middle and left lower lobes (*stars*). Some patchy lobular areas of air trapping are also visible in the right lower and left upper lobes. Cystic bronchiectasis is present in the right middle lobe (*arrow*)

any bronchial obstruction, or in patients with asthma, COPD, emphysema, and sarcoidosis [29, 30, 31].

Expiratory CT technique

The most commonly used technique for the assessment of air trapping at CT is based on postexpiratory thin-section CT scans, obtained during suspended respiration following a forced exhalation. The postexpiratory scans are invariably obtained in conjunction with a routine examination obtained at full inspiration, with scans at spaced intervals from the lung apices to bases. Postexpiratory scans at four to five levels are commonly used. Each of the postexpiratory scans is compared with the inspiratory scan that most closely duplicates its level in order to detect air trapping. Dynamic CT acquisition during continuous expiration, which can be used to collect data at a fixed level during expiration, is the second technique available. Electron-beam CT initially was performed with a scanning time of 100 ms per image to assess the dynamic changes in lung attenuation and in architecture during expiration, with minimal motion artifacts [32]. More recently, a dynamic expiratory maneuver performed during helical CT acquisition was described in a small number of patients with good results in spite of a longer scanning time per image [33]. Motion artifacts, which increase as temporal resolution decreases, represent the major limitations of continuous expiratory CT. The use of 180° linear interpolation algorithms with a 0.5-s rotation time provides images representing scanning periods of approximately 250 ms. Motion artifacts are at maximum during the early phase of expiration and at a minimum during its late phase, which thereby allows good visualization of lobular air trapping with helical CT. With Lucidarme et al. we compared continuous expiratory CT performed with helical scanner and suspended end-expiration CT for the assessment of air trapping in a series of 49 patients who had a chronic airway disease [34]. For the 39 (80%) of those 49 patients with areas of air trapping on at least one expiratory CT scan the air trapping extent and the relative contrast scores obtained with continuous expiratory CT were significantly higher than those obtained with suspended end expiratory CT (Fig. 12a). The improvement provided by continuous expiratory CT can be explained by a small increase in the degree of expiration, which leads to a better detection of air trapping. Patients can have greater

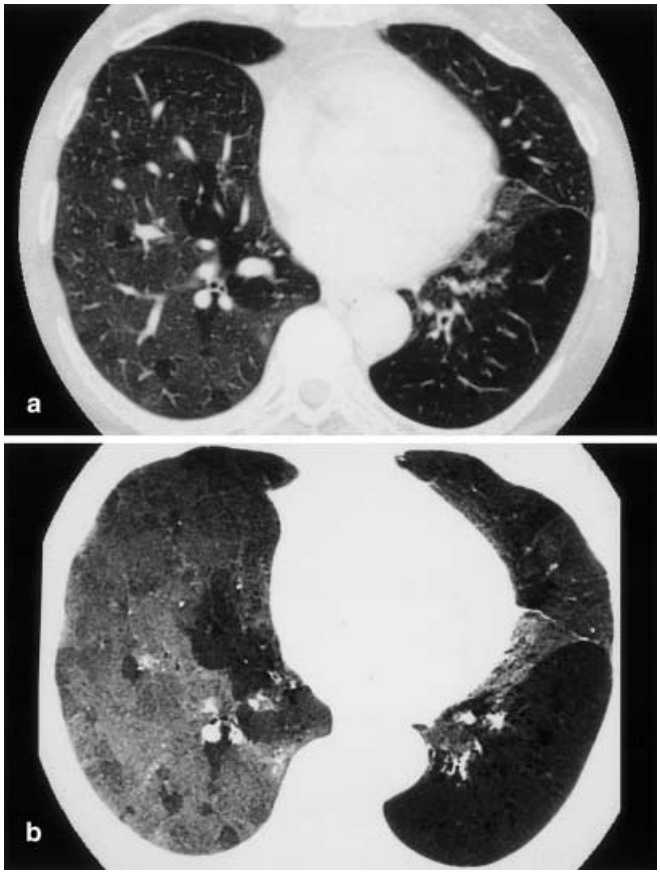

Fig. 12a, b Continuous expiratory CT in a case of postinfectious constrictive bronchiolitis. **a** Thin-section expiratory scan acquired with helical CT acquisition during continuous expiratory maneuver, showing air trapping in the postero- and laterobasal segments of the left lower lobe. Multiple lobular areas of air trapping are also visible in the right lower lobe and lingula. **b** Minimal intensity projection in axial direction obtained from the data set (10-mm-thick volume scanned with helical acquisition and 1.5-mm collimation) increasing the contrast in attenuation between the areas of air trapping and normal parenchyma

difficulty maintaining the residual volume after an exhalation than during an active exhalation when they have to continue the expiratory effort until the end of the acquisition [34]. On the basis of this information, when suspended end-expiration CT images are ambiguous or when patients have difficulty performing the suspended end-expiration maneuver adequately, complementary continuous expiratory CT can be performed with a helical scanner to improve the conspicuity and the apparent extent of air trapping at a given anatomic level. Using low-dose CT, this technique has become routine in some institutions to depict air trapping [35].

Lateral decubitus CT has been proposed as a helpful alternative in the detection and visualization of air trapping in a small number of patients with suboptimal, inconclusive, or uninterpretable supine expiratory CT scans. Lateral decubitus positioning causes the dependent hemithorax to be relatively splinted, thereby restricting movement of the thoracic cage on that side. The lateral decubitus position allows the observer to take advantage of gravitational gradients, thereby accentuating the differences in lung attenuation [36].

Thin-section CT signs of expiratory air trapping can be enhanced with image postprocessing, particularly by using minimal intensity projection technique after helical CT acquisition with thin collimation at suspended expiration. Minimum intensity projection images are associated with increased observer confidence and agreement as compared with thin-section CT alone (Fig. 12b) [37].

Extent of air trapping

The extent of air trapping present on expiratory scans can be measured using a semi-quantitative scoring system which estimates the percent of lung that appears abnormal on each scan. In the scoring system proposed by Stern et al estimates of air trapping were made at each level and for each lung on a four-point scale: 0=no air trapping; 1=1–25%; 2=26–50%; 3=51–75%; and 4= 76–100% of cross-section areas of lung affected [32]. The air-trapping score is the summation of these numbers for the different levels studied. According to Ng et al. this scoring system allows good interobserver agreement [38]. An automatic technique may also be used to obtain an accurate and reproducible assessment of extent of air trapping. By thresholding at –900 HU all the pixels included in areas of air trapping may be highlighted and automatically counted. This permits to calculate the pixel index that is defined as the percentage of pixels in both lungs on a single scan that shows an attenuation lower than a predetermined threshold value [39]. Using multislice CT with 1-mm slice thickness over the lungs performed at full expiration, an exhaustive assessment of the volume of air trapping may be provided as well as a 3D visualization of distribution of air trapping. Acquisition performed at maximum expiration can be insured by spirometrically triggering CT scans at 10% of the vital capacity. Using this method, quantitative assessment of CT images with respect to lung attenuation, lung cross-section surface, or lung volume can be performed with excellent precision [40].

Tracheobronchial stenoses

Helical CT can improve detection, evaluation of extent, and characterization of tracheal or bronchial stenosis. It may orientate the endoscopist and serve as a guide for the taking of a biopsy specimen.

Detection

Computed tomography has proven to be a reliable method to demonstrate tumoral lesions of the proximal airways including those located beyond the bronchoscopic range [41, 42]. Although unable to demonstrate early mucosal changes, bronchitis, squamous metaplasia, and benign papillomas, all found at bronchoscopy, helical CT is recommended to be performed prior to bronchoscopy for all patients with unexplained hemoptysis [43, 44].

Extent

Multiplanar reformations, 3D images of bronchial tree, and virtual endoscopy may prove valuable in patients with tracheal or bronchial stenosis from central tumors as well as from inflammatory diseases or fibrosis after surgery or interventional endoscopic or radiologic treatment (Figs. 1, 4). Main clinical applications include localization and measurement of bronchial stenosis [45]. Imaging may contribute to image guidance of endobronchial treatment modalities such as endobrachytherapy, laser treatment planning, or endoprothesis. Imaging is also helpful in the follow-up after such treatment to search for complications such as recurrence of stenosis, stent misplacement, or displacement. It provides information that allows to direct a more focused real bronchoscopy, including demonstration of the length of a stricture and depiction of additional areas of strictures beyond an area of narrowing that is not traversable by the bronchoscope. This capacity is particularly important in patients who are prone to multiple strictures such as those with Wegener's granulomatosis or relapsing polychondritis (Fig. 13) [45]. It may also be easier to measure the degree of stenosis at CT compared with the view obtained at bronchoscopy. Whereas the extraluminal extent of an abnormality is not visible at bronchoscopy, it can generally be demonstrated at CT. In addition, imaging may help to precisely visualize the attachment site of

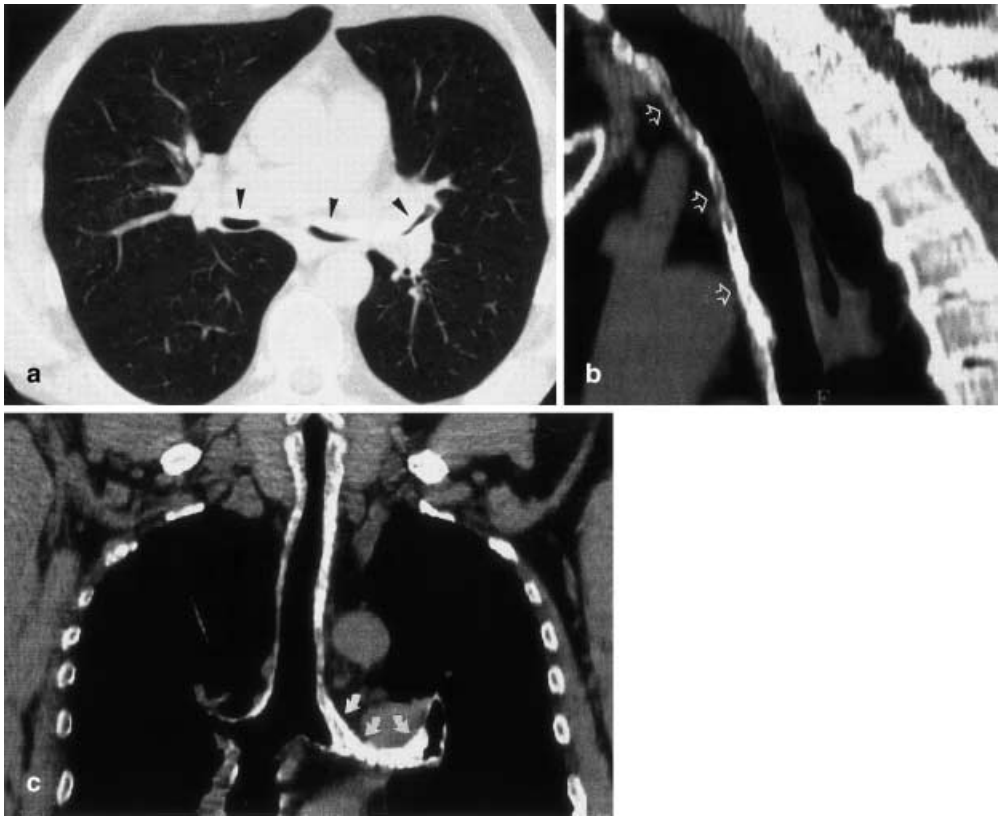

Fig. 13a–c Relapsing polychondritis. **a** Axial thin-section scan showing a reduction of the lumens of the right intermediate bronchus and left main bronchus and a stenosis of the left upper lobar bronchus with calcified abnormal thickening of the anterior wall of the airway (*arrowheads*). **c** Coronal reformation image showing thickening of the lateral walls of the trachea containing multiple calcified deposits and calcified thickening of the walls of the left main bronchus (*curved white arrows*) inducing stenosis of the left main bronchus and occlusion of the left upper lobar bronchus. **b** Sagittal reformatted image showing abnormal thickening partially calcified of the anterior wall of the trachea (*open arrows*)

a benign bronchial tumor which can strongly influence the surgical decision making [7].

Characterization

Analysis of the shape, content, density, and anatomic relationships of the lesion on the successive contiguous CT images can contribute to determining the precise etiology of a bronchial stenosis. Focal or diffuse fat infiltration visible within an endoluminal bronchial mass is characteristic of hamartoma [46]. The association with central or popcorn calcification reinforces this diagnosis. Broncholithiasis, a condition in which peribronchial calcified nodal disease erodes into or distorts an adjacent bronchus, is recognized at CT by the presence of a calcified endobronchial or peribronchial lymph node, associated with bronchopulmonary complication due to obstruction (including atelectasis, pneumonia, bronchiectasis, and air trapping), in the absence of an associated soft tissue mass [47]. Focal or diffuse bronchial stenosis can be observed in several inflammatory diseases, such as sarcoidosis, Wegener's granulomatosis, amyloidosis, and relapsing polychondritis (Fig. 13) [48, 49]. Computed tomography can demonstrate regular or irregular narrowing of the airways, thickening of the bronchial wall, sometimes with dense calcium deposits, or extrinsic airway compression by enlarged nodes.

Guiding bronchial or transbronchial biopsy

When bronchial tumors are not visible at endoscopy, CT can be useful to guide the taking of bronchial or transbronchial biopsy by showing the relationships between the bronchial tree and peripheral carcinomatous lesions [43, 50]. The ability to make a definite diagnosis after bronchial forceps biopsy and bronchial brushing has proven to be better for lesions characterized by a bronchus cutoff or bronchus contained within a tumor. Transbronchial needle aspiration has proven to be best able to provide a diagnosis in patients with a bronchus compressed by the tumor or with a thickening and narrowing of the bronchus leading to the tumor [50].

Airway fistula and dehiscence

Helical CT with thin collimation is the most accurate technique to identify peripheral bronchopleural fistulas that are most commonly caused by necrotizing pneumonia or secondary to traumatic lesions [51]. Nodobronchi-

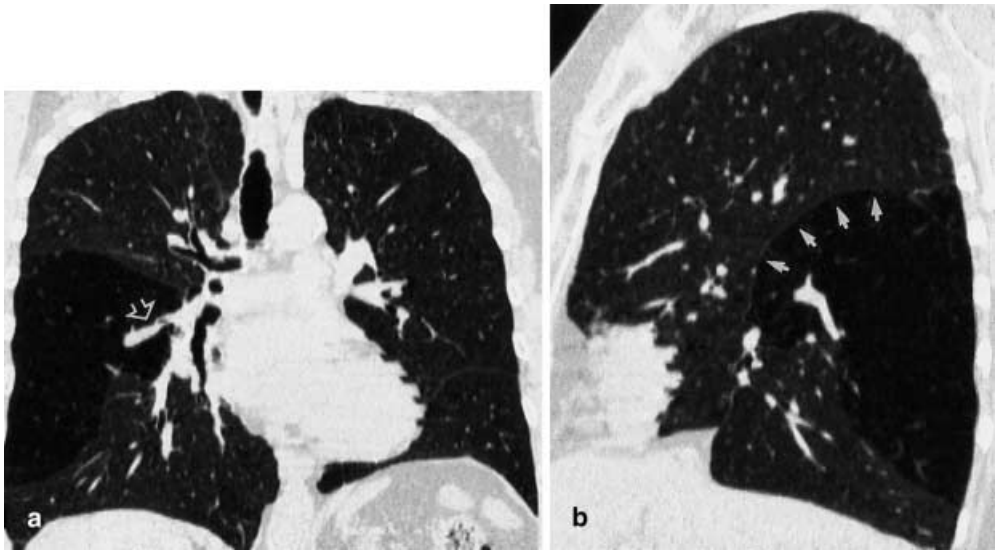

Fig. 14a, b Bronchial atresia of the segmental bronchus of the upper segment of the right lower lobe. **a** Coronal and **b** sagittal reformatted images after multislice CT acquisition and thin-slice thickness. Decreased lung attenuation and perfusion of the upper segment of the right lower lobe is associated with a hyperinflation of that segment as shown by the bulging of the right major fissure (*white arrows*). The right parahilar tubular opacity (*open arrow*) reflects the bronchocele beyond the atretic bronchial segment

al and nodobronchoesophageal fistulas that are most commonly caused by *Mycobacterium tuberculosis* infection are depicted by the presence of gas in cavitated hila or mediastinal lymphadenopathy adjacent to the airways. Direct visualization of the sinus tract between the bronchial lumen and the hypertrophied cavitated lymph node and/or the esophagus can be helpful in planning therapy. Tracheal diverticula and tracheo-broncho-esophageal fistula may also be diagnosed even in adults (Figs. 3, 8) [52].

Computed tomography has a high degree of sensitivity and specificity for depicting bronchial dehiscence occurring after lung transplantation [53]. Bronchial dehiscence is seen as bronchial wall defect associated with extraluminal air collections. Schlueter et al. showed that in patients with small dehiscences (<4 mm) and patients with a tiny or small amount of extraluminal air, the anastomosis tends to heal without sequela [54]. When patients have larger amounts of extraluminal air or larger (>4 mm) dehiscences at presentation, CT cannot help predict which patients will require intervention [54].

Congenital abnormalities of the airways

Helical CT easily detects as an asymptomatic incidental finding congenital anomalies of the bronchial branching pattern such as ectopic bronchi, supernumerary anomalous bronchus, bronchial atresia, and lobar hypoplasia [55, 56]. A focal mucoid impaction projecting into a hyperinflated and oligemic segment or lobe is highly suggestive of the diagnosis of bronchial atresia. Segmental or lobar hyperinflation distal to the atretic bronchus which develops early in life as a result of collateral ventilation is easily identified on CT scans, whereas the bronchoscopy is usually interpreted as being normal (Fig. 14) [57]. Multiplanar reformation enables the visualization of the linear opacity connecting the bronchocele and the bronchial tree corresponding to the atretic bronchial segment [57].

Hemoptysis or recurrent infection, as secretions can be retained with resultant inflammation and hypervascularity, can reveal an ectopic bronchus, particularly the tracheal bronchus or accessory cardiac bronchus which are easily analyzed by CT using cine viewing, multiplanar reformation, and 3D techniques [55].

Bronchiectasis

In spite of its decreased prevalence in developed countries, bronchiectasis remains an important cause of hemoptysis and chronic sputum production. The CT cardinal sign of bronchiectasis is dilatation of the bronchi with or without bronchial wall thickening. The CT criteria for diagnosing cylindrical bronchiectasis include a bronchial diameter greater than that of the accompanying pulmonary artery, lack of tapering of the bronchial lumen, and visualization of a bronchial lumen within 1 cm of the costal pleura or a bronchus abutting the mediastinal pleura (Figs. 15, 16) [58]. Varicose bronchiectasis is characterized by a beaded appearance when bronchi lie parallel to the scanning plane. Cystic bronchiectasis is seen as thin-walled cystic spaces that may contain fluid levels. The topographic distribution of cystic spaces along a segmental distribution permits to differentiate bronchiectasis from the other cystic lesions. Strings of cysts set in line from the hilum to peripheral lung zones or joined cysts abutting the mediastinal pleura or the vertebral pleura within completely collapsed lobes or seg-

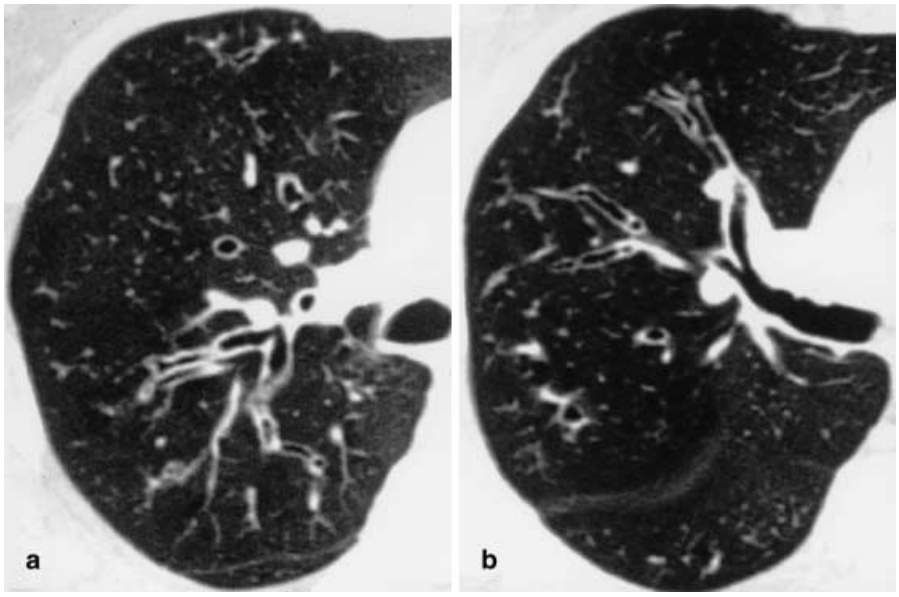

Fig. 15 Cylindrical bronchiectasis in the right **a** upper and **b** middle lobes. Axial 2.7-mm-thick slices after helical CT acquisition showing the lack of tapering of subsegmental bronchi

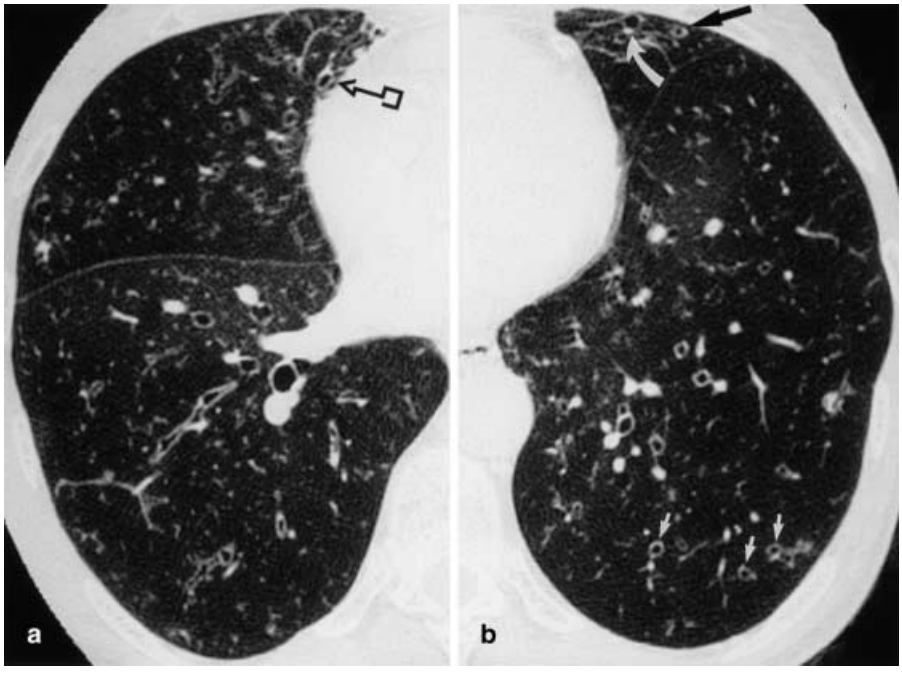

Fig. 16a, b Cylindrical bronchiectasis. Axial thin-section scans targeted on the **a** right and **b** left lungs. Cylindrical bronchiectasis is recognized on the basis of the visibility of bronchial lumens abutting the mediastinal pleura (*open arrows*) in the right middle lobe, and bronchial lumen within the 1-cm from the costal pleura (*black and curved white arrows*) in the lingula. The signet ring sign is also present in the posterobasal segment of the left lower lobe (*white small arrows*)

ments are particularly suggestive of bronchiectatic airways (Fig. 11). Secretion accumulation within bronchiectatic airways is generally easily recognizable as lobulated glove-finger, -V or -Y shaped densities. Typically, the diagnosis of dilated bronchi filled with pus, secretions, or mycetoma, is based on the recognition on a few successive slices of the segmental distribution of the corresponding densities and the observation of the homologous pulmonary arteries, whose diameters are smaller than those of the dilated filled bronchi (Fig. 17) [59]. The pattern and distribution of abnormalities revealed by CT in patients with bronchiectasis are influenced by the underlying cause. Although the correct diagnosis may be suggested on the basis of CT findings in many cases, considerable overlap in the pattern and distribution of bronchiectasis was found between the diseases [60, 61].

Thin-section CT has proven to be a reliable and non invasive method for the assessment of bronchiectasis and has largely eliminated the need for bronchography [62]. Although thin-section CT with 10-mm intervals allows

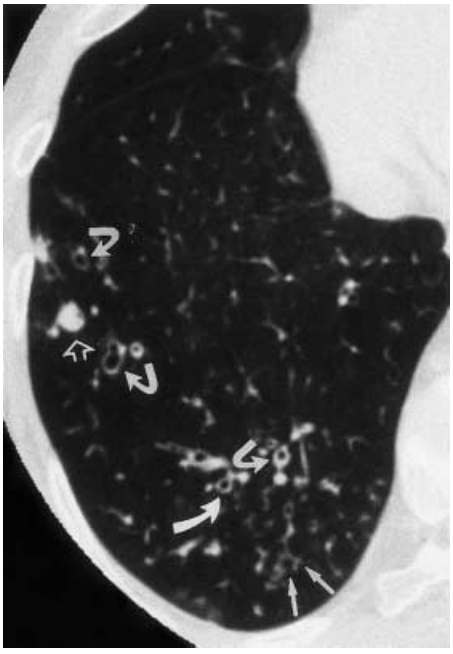

Fig. 17 Bronchiectasis and inflammatory bronchiolitis. Thin axial CT section targeted on the right lung. Cylindrical bronchiectasis is present in basal segments of the right lower lobe (*curved arrows*). Mucoid impaction in a dilated bronchus taken a nodular appearance (*open arrow*) is also present. Small centrilobular nodular and linear branching opacities (tree-in-bud sign) are visible in the posterobasal segment (*white arrows*)

confident diagnosis of the presence and extent of bronchiectasis in the majority of patients, several limitations of the technique need to be recognized [63, 64]. These limitations include:

1. Artifacts resulting from both respiratory and cardiac motion
2. Overlooking of areas of focal bronchiectasis located exclusively in skipped areas
3. Difficulty of perceiving the slight dilatation of mild cylindrical bronchiectasis

Motion degradation of bronchial images can be reduced by using a 180° interpolation algorithm to reconstruct axial images after helical scanning. Electrocardiographic gating can be used to reduce cardiac motion artifacts that may mimic disease [65]. In addition, volumetric helical acquisition during breath holding eliminates the potential risk of missing small subtle bronchiectasis in areas skipped by the interspacing between thin-section CT scans (Fig. 15) [66]. Because of many factors that can cause transient or permanent changes in diameter of the relatively compliant pulmonary arteries, invalidating the finding of cylindrical bronchiectasis based on the bronchoarterial diameter ratio >1, the lack of tapering of bronchial lumen has proven to be the most reliable sign of cylindrical bronchiectasis [64]; however, this finding is difficult to perceive on successive spaced thin-section CT scans and its assessment is significantly improved by using helical CT with thin collimation and viewing the contiguous scans in a cine mode. As mucoid impaction filling bronchiectatic bronchi can simulate pulmonary

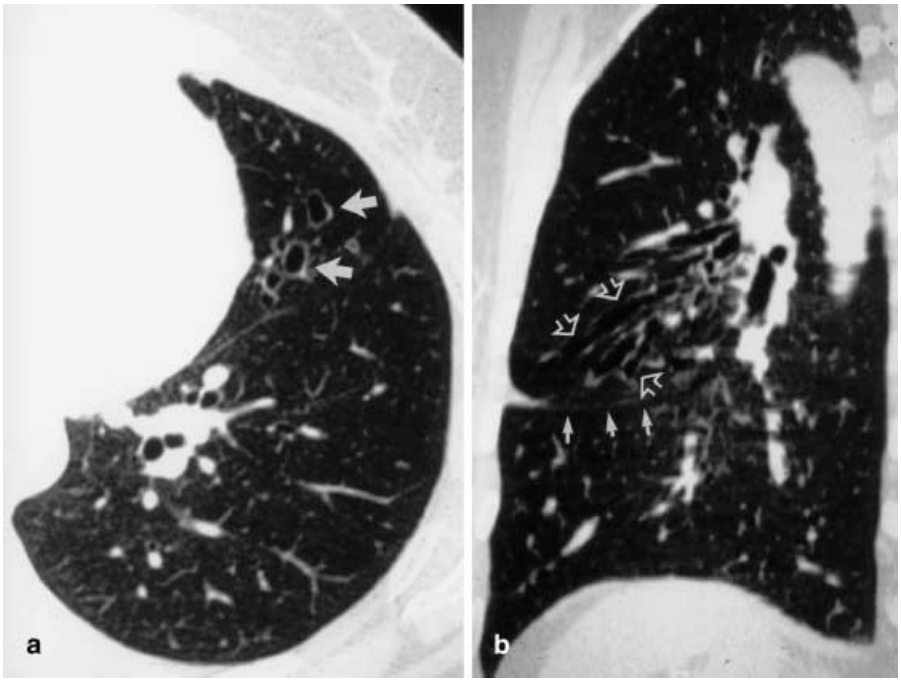

Fig. 18a, b Focal bronchiectasis in the lingula. **a** Thin axial section showing varicose bronchiectasis in the lingula. **b** On the reformatted sagittal oblique image dilated bronchi (*open arrows*) are seen within both segments of the lingula that is partly collapsed as emphasized by the ascension of the lower part of the fissure (*small white arrows*)

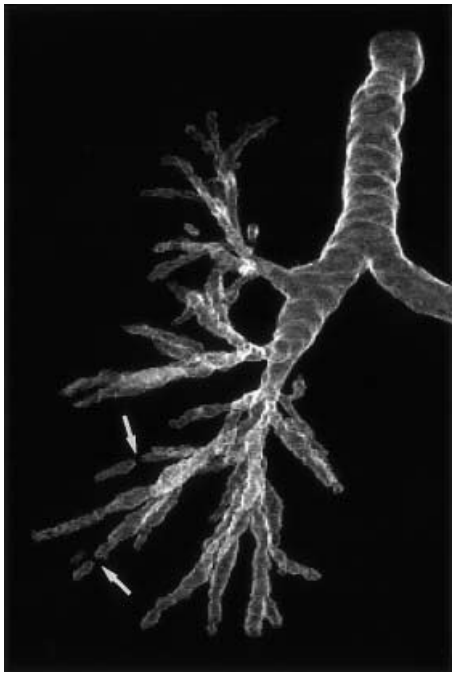

Fig. 19 Bronchiectasis on a virtual bronchogram. Coronal view of virtual bronchography after multislice CT acquisition and thin slice thickness targeted on the right lung. Cylindrical bronchiectasis is seen involving several bronchi in the right middle and lower lobes. Irregularities in bronchial caliber are well displayed. Discontinuities in bronchial lumen (*arrows*) reflect the filling of bronchial lumen by retained secretions

nodules or masses on a single thin-section CT scan and pulmonary arteries are not recognized because of intense vasoconstriction in hypoventilated areas (Fig. 17), helical CT with thin collimation provides a multiplanar display of the radiopaque tubular structures converging toward the hilum in a segmental or subsegmental distribution, corresponding to bronchiectasis.

Lucidarme et al. compared helical CT acquisition with 3-mm collimation and thin-section CT scans with 10-mm intervals in a series of 50 consecutive patients with suspicion of bronchiectasis [66]. The presence of bronchiectasis was noted in 22 patients and 70 segments on thin-section CT scans with 10-mm interval and in 26 patients and 90 segments with helical CT scanning [66]. The interobserver agreement was significantly better with helical CT than with thin-section CT scans for the presence or absence of bronchiectasis on a per-segment basis, and also for assessing the extent of bronchiectasis in a given lobe and the distribution of disease in a given segment [66]. Such an accurate assessment of extent of disease is particularly required before surgery for focal bronchiectasis (Fig. 18). Indeed, the surgeon must identify with certainty which segments are diseased, since surgical techniques frequently permit preservation of one or more normal pulmonary segments from a lobe in which bronchiectasis is present. For all these reasons, multislice CT with thin-slice thickness using low dose should become the recommended routine protocol for the diagnosis and assessment of bronchiectasis. In addition, virtual bronchography reconstructed after multislice CT acquisition with thin-slice thickness should permit to increase the confidence level of diagnosis of mild cylindrical bronchiectasis or to improve the differential diagnosis between cystic bronchiectasis and lung cysts (Fig. 19) [10, 11].

Small airway disease

The diagnosis of small airway disease is challenging for the clinician, as there is no pathognomonic clinical and functional feature. The chest radiograph is normal or may show non-specific findings. Thin-section CT scan is currently the best imaging technique for assessment of diseases of the small airways [67]. As the normal bronchioles measure less than 1 mm in diameter and have a wall thickness of less than 0.1 mm, they are below the limit of visibility on thin-section CT scans and thus are too small to be visualized. The fact that bronchioles are centrilobular structures being clustered near the center of a secondary pulmonary lobule accounts for the characteristic centrilobular distribution of bronchiolar abnormalities on thin-section scan.

For the pathologist, small airway disease has the same meaning as bronchiolitis. The current pathologic classification divides bronchiolitis into three main categories: cellular bronchiolitis; bronchiolitis obliterans with intraluminal polyps; and constrictive (obliterative) bronchiolitis.

Cellular bronchiolitis

Cellular bronchiolitis is characterized by inflammatory cellular infiltrates that involve the lumen and/or the wall of bronchioles. It is seen in various infections including bacterial, viral, mycoplasma pneumonia, invasive airway aspergillosis, as a result of toxic fumes inhalation, or in association with chronic airway disease, such as bronchiectasis, asthma, and COPD, or distal to any obstructive bronchial lesion. Other conditions may also feature a cellular bronchiolitis (follicular bronchiolitis, respiratory bronchiolitis, hypersensitivity pneumonitis, diffuse panbronchiolitis, and diffuse aspiration bronchiolitis) [68, 69, 70, 71].

Thin-section CT findings consist predominantly of centrilobular nodular and branching linear opacities. The association of both nodular and linear branching opacities gives the “tree-in-bud” appearance (Fig. 17) [72]. These abnormalities represent enlarged bronchioles filled with mucous or pus coursing perpendicular and parallel to the CT plane of section. The centrilobular nodules may have

Fig. 20 Respiratory bronchiolitis in a heavy smoker. Thin-section CT scan targeted on the right lung showing small ill-defined centrilobular nodules associated with ground-glass opacities that reflect macrophage accumulation in the distal air spaces and bronchioles

either well-defined and regular-shaped margins, and are of soft tissue density, or have only poorly defined margins and are of hazy density. Some nodules may appear larger and ill-defined in contours, reflecting the extent of the inflammatory lesions to the adjacent peribronchiolar air spaces. Linear branching centrilobular opacities without nodules have the same meaning as tree-in-bud sign. Although less specific, small centrilobular nodules without linear opacities can also be seen in cellular bronchiolitis [73]. Small, ill-defined centrilobular nodules, homogeneously and diffusely distributed throughout the lungs, is a pattern highly suggestive of hypersensitivity pneumonitis [74]. Small, ill-defined centrilobular nodules more or less associated with bronchial wall thickening and centrilobular emphysema and ground-glass attenuation in heavy smokers is highly suggestive of respiratory bronchiolitis (Fig. 20) [75].

Cellular bronchiolitis, depending on its cause, may recover under specific or anti-inflammatory treatment or be followed by one of the two types of bronchiolitis obliterans.

Bronchiolitis obliterans with intraluminal polyps

Histologically, bronchiolitis obliterans with intraluminal polyps is characterized by polypoid endobronchial connective tissue masses (composed of myxoid fibroblastic tissue) that appear to float freely within a bronchiolar lumen or be only focally attached to the wall. In many cases the fibroblastic proliferation is continuous with a similar process in the more distal air spaces called organizing pneumonia. When patchy organizing pneumonia is present, the two lesions are combined in the name bronchiolitis obliterans with organizing pneumonia (BOOP). Bronchiolitis obliterans with intraluminal polyps is a common reparative reaction that occurs in numerous settings (infection, toxic fumes inhalation, radiation or drug therapy), whereas idiopathic BOOP, named cryptogenic organizing pneumonia (COP), is currently regarded as an idiopathic interstitial pneumonia instead of an airway disease [76].

When organizing pneumonia is present, the main CT findings include unilateral or bilateral areas of air-space consolidation [77, 78]. The distribution of abnormalities may be predominantly subpleural or peribronchial. Such distribution is also found when air-space consolidation takes the appearance of large nodular opacities with irregular margins, containing air bronchogram associated with relatively broad pleural and parenchyma bands [79]. When organizing pneumonia is absent, the CT findings consist of centrilobular nodular opacities that may reflect the presence of intrabronchiolar granulation tissue polyps or peribronchiolar consolidation.

In most of the cases bronchiolitis obliterans with intraluminal polyps is well responsive to steroids. Although many of the causes of bronchiolitis obliterans with intraluminal polyps are similar to those of constrictive bronchiolitis the former evolving into the latter is rarely documented.

Constrictive bronchiolitis

Constrictive (obliterative) bronchiolitis is characterized mainly by concentric narrowing of the bronchioles caused by submucosal and peribronchiolar irreversible fibrosis. The lesions may extend along the long axis, impairing in this way the collateral ventilation and causing an obstruction to the air flow. It may be seen as the result of childhood viral infection, mycoplasma pneumonia, or toxic fume inhalation, in association with bronchiectasis, cystic fibrosis, and bronchopulmonary dysplasia. It is one more common pulmonary complication in patients with rheumatoid arthritis, particularly those treated with penicillamine [67]. It is a manifestation of chronic graft-vs-host disease following bone marrow transplantation and chronic rejection after heart–lung transplantation [80]. It is rarely seen in association with inflammatory bowel disease. It has been described in association with pulmonary neuroendocrine cell hyperplasia, and as a result of ingestion of sauropus androgynus [67, 81, 82].

Obstruction of the bronchiolar lumen results in hypoxia of the underventilated lungs, reflex vasoconstriction, and air trapping. On CT scans the combination of local vasoconstriction and air trapping results in decreased attenuation of the affected areas of the lung. There is associated blood flow redistribution to areas of normal lung that are therefore of higher attenuation. These changes are usually patchy in distribution and result in adjacent areas of abnormal low attenuation lung and relatively overperfused higher attenuation normal lung. This combination is referred to as mosaic perfusion. Although the mosaic perfusion CT pattern can also be caused by primary pulmonary arterial abnormalities, such as pulmonary arterial hypertension and chronic pulmonary thromboembolism, in patients with small airway diseases, the regional differences in lung attenuation and lung perfusion are increased on expiratory scans due to air trapping (Figs. 11, 12) [26, 83].

Occasionally lesions of constrictive bronchiolitis may be seen predominantly affecting one lung as is characteristic in Swyer James syndrome which is a variant of constrictive bronchiolitis due to viral bronchiolitis occurring in childhood or infancy. Thin-section CT findings include unilateral lung hypoattenuation, thin-walled bronchiectasis, and air trapping. Most often, similar changes are present in the other lung but to a lesser extent [84].

In case of more global involvement of the small airways, the lack of regional homogeneity of the lung density is difficult to perceive on inspiratory scans. Mosaic perfusion becomes visible only on expiratory scans. In patients with particularly severe and widespread involvement of the small airways, inspiratory scans appear with an apparent uniformity of decreased attenuation in the lungs, and scans taken at end expiration may appear unremarkable [83]. In these patients the most striking features are paucity of pulmonary vessels and lack of change of the cross-section areas of the lung at comparable levels on inspiratory and expiratory scans (Fig. 21). In such a situation the distinction between constrictive bronchiolitis and panlobular emphysema may be difficult on the basis of CT appearances alone.

The clinical course of constrictive bronchiolitis is highly variable. The majority of cases of postviral constrictive bronchiolitis are self-limiting with no long-term consequences. In contrast, patients with constrictive bronchiolitis in association with rheumatoid arthritis and some patients developing constrictive bronchiolitis following heart–lung transplantation often have a more rapidly progressive disease with survival measured in months rather than in years [67, 85].

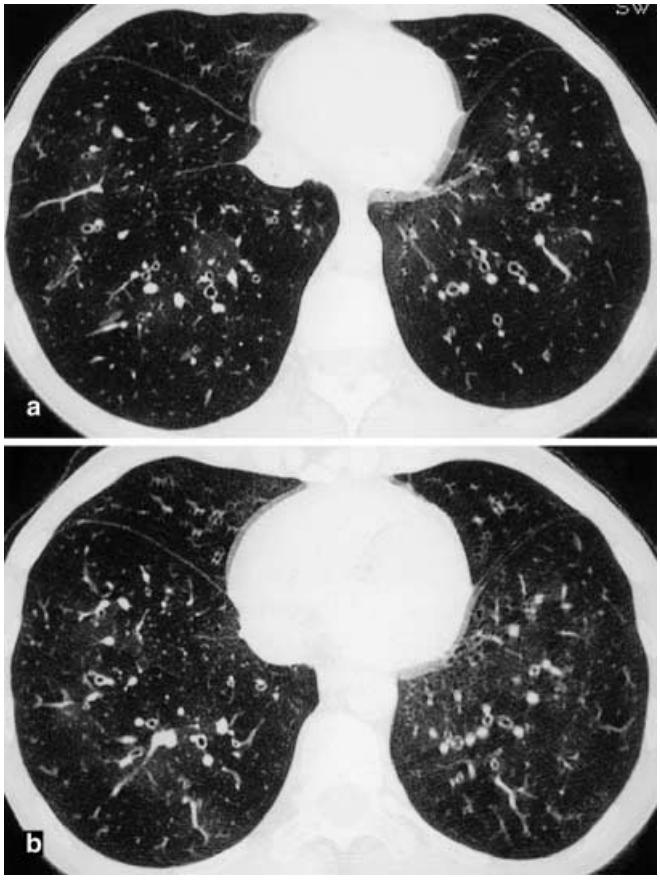

Fig. 21 Diffuse constrictive bronchiolitis. **a** Inspiratory and **b** expiratory thin-section scans in a patient with chronic obstructive lung disease due to constrictive bronchiolitis. Mosaic perfusion pattern is present in both scans but difficult to perceive. Decreased lung attenuation and oligemia is diffuse in distribution on both inspiratory and expiratory scans. Note the lack of change of the cross-sectional areas of the lungs at comparable level on inspiratory and expiratory scans

CT air trapping and pulmonary function

The extent of air trapping rather than the lung attenuation better predicts pulmonary function tests findings of obstruction. Although abnormal expiratory air trapping may be depicted in patients with normal pulmonary function tests, significant correlations have been shown between extent of air trapping at expiratory CT and indices of air-flow obstruction at pulmonary function tests in patients with various types of small airway disease, including constrictive bronchiolitis, and hypersensitivity pneumonitis [81, 86, 87, 88, 89]. The CT features of small airway diseases are common findings in patients with bronchiectasis, and a recent work has suggested that the extent of CT evidence of small airway disease (decreased lung attenuation and expiratory air trapping) is the major determinant of air-flow obstruction. In contrast, the obstructive defect found at pulmonary function tests was not related to the degree of collapse of large airways on expiratory CT or the extent of mucous plugging of the airways [90].

Chronic obstructive pulmonary disease

Involvement of proximal airways includes bronchial wall thickening, saber-sheath trachea, and expiratory airway collapse due to abnormal flaccidity.

Bronchial wall thickening

Bronchial wall thickening is commonly present on thin-section CT scans of patients with COPD. It is considered to be related to chronic bronchitis [91].

Saber-sheath trachea

The saber-sheath trachea is a deformity defined as excessive coronal narrowing of the intrathoracic trachea in tandem with widening of the sagittal tracheal diameter. In pronounced examples the tracheal index (coronal–sagittal diameters ratio) can be less than 0.6. Concurrently, the cross-sectional diameter of the trachea decreases to less than 60% of normal [92]. This deformity is highly characteristic of COPD. It affects primarily the intrathoracic trachea and the main bronchi and usually spares the cervical trachea, which retains normal dimensions and a normal configuration. The tracheal wall is slightly thickened, rigid, smooth, or slightly corrugated with occasional ossification or calcification of the cartilaginous elements.

Tracheobronchomalacia

Tracheobronchomalacia is another abnormality that can also occur in patients with COPD. The increase in compliance is due to the loss of integrity of the wall's structural components and is particularly associated with damaged or destroyed cartilages. The coronal diameter of the trachea becomes significantly larger than sagittal one, producing a lunate configuration to the trachea. The flaccidity of the trachea or bronchi is usually most apparent during coughing or forced expiration. In patients with COPD with high downstream resistance, particularly high dynamic pressure gradients can be generated across the tracheal wall, and it is likely that caliber changes of more than 50% can occur at expiration with normal tracheal compliance. As a result, only a decrease in cross-section area of the tracheal lumen greater than 70% at expiration indicates tracheomalacia [32]. Dynamic expiratory multislice CT may offer a feasible alternative to bronchoscopy in patients with suspected tracheobronchomalacia. Dynamic expiratory CT may show complete collapse or collapse of greater than 75% of airway lumen (Fig. 22). Involvement of the central tracheobronchial tree may be diffuse or focal. The reduction of airway may have an oval or crescentic shape. The crescentic form is due to the bowing of posterior membranous trachea [93].

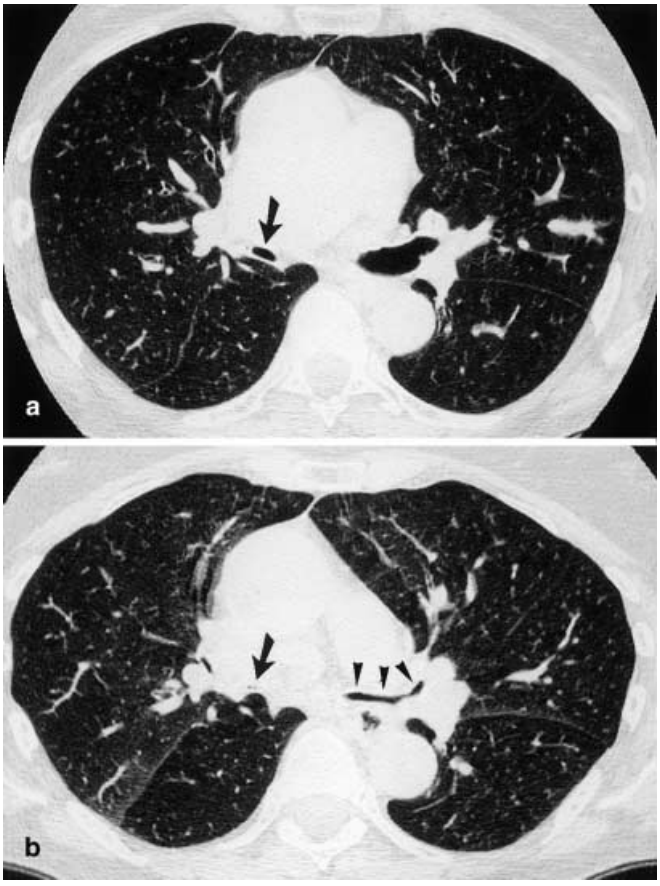

Fig. 22a, b Tracheobronchomalacia. **a** Inspiratory and **b** expiratory thin sections. On the inspiratory scan the lumen of the right intermediate bronchus is reduced (*arrow*), whereas the lumen of the main and upper lobar bronchi is normal. On expiratory scan (**b**), the lumen of the right intermediate bronchus is completely collapsed, whereas the reduction in caliber of the left main and upper lobar bronchi is >70%

Involvement of distal airways

Involvement of distal airways is commonly present in patients with COPD. Small centrilobular nodules or linear branching opacities may represent mucous plugging of bronchioles and small bronchi more or less associated with inflammatory bronchiolitis. These abnormalities are non-specific of COPD and can also be present on thin-section CT scans of cigarette smokers (respiratory bronchiolitis) before the development of COPD (Fig. 20) [94, 95]. These abnormalities could be the precursors of small airway obstruction and of centrilobular emphysema but they can disappear if the patient stops smoking [95].

Expiratory air trapping

As with other airway diseases, COPD may result in expiratory air trapping [91]. Using CT scans performed at 10% of vital capacity, Lamers et al. showed that patients with chronic bronchitis had lower attenuation than that of normal individuals. This lower attenuation at expiration was considered as a finding of bronchiolar lumen obstruction [96]. When emphysema is present, air trapping can be due to either airway obstruction caused by a loss of alveolar attachment to the airways directly related to emphysema, or to intrinsic bronchial or bronchiolar abnormalities associated with cigarette smoking. Gevenois et al. demonstrated in patients with emphysema that thin-section CT scans obtained at the end of maximum expiration (10% of vital capacity) and a threshold attenuation value of –910 HU provided better correlation with measurement of air-flow obstruction at pulmonary function tests than did thin-section CT scans obtained at full inspiration (90% of vital capacity) and using a –950 HU threshold [97]. This finding probably reflects air trapping due to airway obstruction at expiration rather than reduction of the alveolar wall surface. By contrast the use of –950 HU threshold on inspiratory scans provides the best correlation with the extent of emphysema [98].

Asthma

Asthma is a chronic inflammatory condition involving the airways. The precise component of this inflammation remains to be elucidated and the causes are uncertain. This inflammation of the airways causes increases in the existing bronchial hyperresponsiveness answering to a variety of stimuli. This is commonly used in practice to confirm the clinical diagnosis of asthma. In susceptible individuals, this inflammation induces recurrent episodes of wheezing, chest tightness, breathlessness, and coughing usually associated with widespread but variable airflow obstruction that is often reversible either spontaneously or with treatment. Chronic inflammation process leads to structure changes such as new vessel formation, airway smooth muscle thickening and fibrosis which may result in irreversible airway narrowing. The current therapy is based in most instances on an inhaled steroid as a controller medication (anti-inflammatory). When necessary bronchodilator (β_2 agonist) is used.

The clinical indications for CT in patients with asthma have included to detect bronchiectasis in patients with suspicion of allergic bronchopulmonary aspergillosis (ABPA), to document the presence and extent of emphysema in smokers with asthma, and to identify conditions that may be confused with asthma, such as hypersensitivity pneumonitis [99]. The CT abnormalities on airway and lung parenchyma have been reported in several studies, but only few of them compared the frequency of the findings observed in asthmatics with a control group [100, 101, 102, 103]. Park et al. demonstrated that only three findings were significantly more frequent in asthmatic patients than in normal individuals: bronchial wall thickening; bronchial dilatation; and expiratory air trapping [103]. Bronchial wall thickening is a frequent abnormality related to the severity of asthma [100]. Identification of bronchiectasis in patients with asthma but without ABPA is plausible because bronchiectatic changes are seen at autopsy in patients who have died with long-standing asthma. The true prevalence of bronchiectasis in patients with uncomplicated chronic asthma, however, remains unclear [100, 101, 102]. Mild cylindrical bronchiectasis based on a mild elevation of the bronchoarterial ratio may occur in patients with asthma, due to hypoxic pulmonary vasoconstriction related to localized areas of air trapping [101]. A visual illusion is that thick-walled bronchi appear larger than the adjacent vessel, even if their internal diameters are the same. So mild cylindrical bronchiectasis should be diagnosed with caution in patients with asthma and should not be the sole criterion for suggesting the diagnosis of ABPA in these patients. Abnormal expiratory air trapping has been observed in 50% of asthmatic patients [103]. This reflects the luminal obstruction of the airways and is potentially but not always reversible. Other abnormalities less frequently observed in asthma include mucoid impactions and linear bands reflecting subsegmental atelectasis. They have been proven to be reversible. Centrilobular thickening observed in patients with severe asthma expresses the small bronchial or bronchiolar wall thickening. Focal and diffuse areas of decreased lung attenuation seen in 20–30% of asthmatic patients are likely due to a combination of air trapping and pulmonary oligemia due to alveolar hypoventilation [100, 101].

The real current challenge for CT in asthma is to visualize and quantify the lumen and wall of airway and lung attenuation to assess the extent of airway obstruction, the degree of inflammation in small airways, and to evaluate in vivo the airway wall remodeling. This will become crucial in the monitoring of current and future therapy.

Airway obstruction and hyperresponsiveness

We demonstrated recently that patients with mild intermittent asthma present with baseline bronchoconstriction compared with normal subjects when examined with CT performed at a controlled lung volume (65% of total lung capacity after full inspiration), as they had stopped all treatment 48 h prior to study [24]. This was confirmed by the fact that inhalation of salbutamol after methacholine challenge brought their bronchi not only back to cross-sectional areas comparable to those of the control group, but also above their own baseline values (Fig. 23). This suggests that bronchoconstriction is due

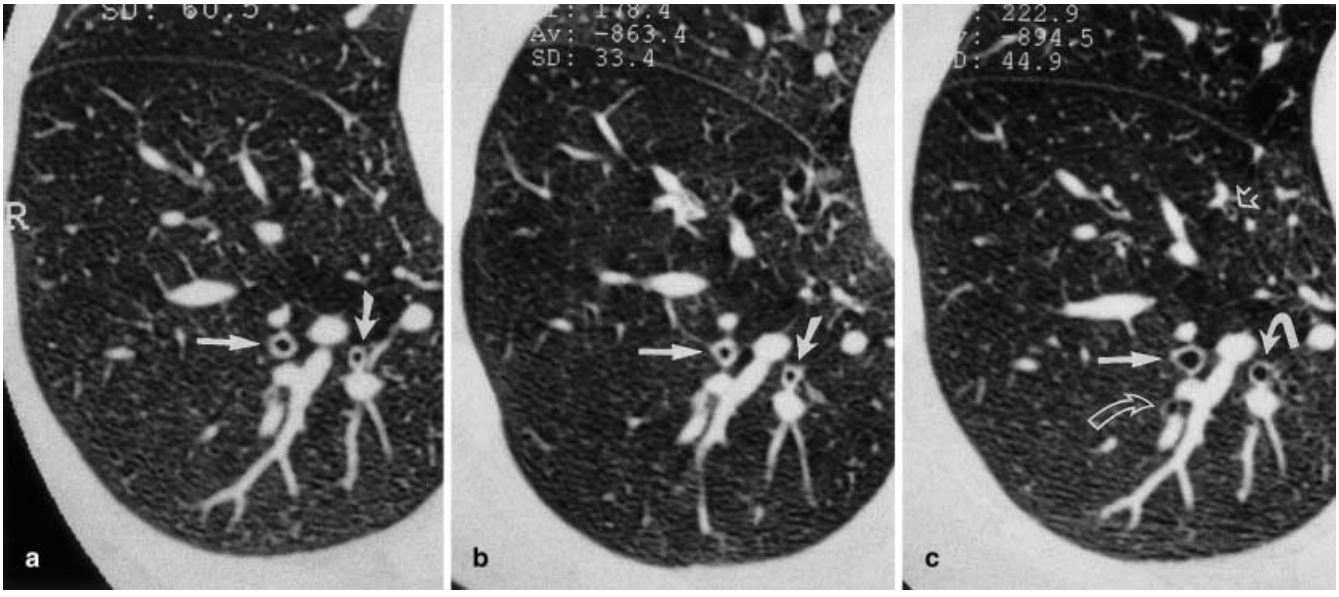

Fig. 23a–c Airway hyperresponsiveness in mild intermittent asthma. Thin-section CT scans targeted on the right lower lobe at 65% of total lung capacity controlled by spirometrical triggering, **a** at baseline, **b** after methacholine inhalation, and **c** 10 mm after salbutamol inhalation. The cross sections of two thick-walled subsegmental bronchi of the posterobasal segment of the right lower lobe (*white arrows*) present with a certain degree of constriction after methacholine (**b**). After salbutamol (**c**), the bronchial lumens dilated and appear larger than before challenge. Other small bronchial lumens (*open arrows*) not previously visible have dilated sufficiently to be depicted after salbutamol

to an increased baseline tone or an impaired stretching in asthmatic patients. In the same study bronchial cross-section area was not influenced by methacholine challenge more in asthmatics than in normal subjects. In addition, the presence of expiratory air trapping, induced by methacholine challenge and partly reversible after salbutamol inhalation in asthmatic patients, confirmed that the methacholine induced bronchoconstriction involves mainly or exclusively the smallest airways [24].

Airway inflammation

Because lung attenuation can be quantified in a reproducible way with CT and values for normal subjects (examined at a controlled lung volume) lie within a normal range, we applied the same approach as Wollmer et al. used to assess various stages of inflammation in smokers [104]. The lung attenuation and anteroposterior attenuation gradient values found for intermittent asthmatic patients at a selected lung volume (65% of total lung capacity), monitored by pneumotachography, were significantly higher than in normal subjects [24]. We hypothesized that the well-known peribronchial and small airway inflammation occurring in asthma explains the attenuation and gradient increases. The observation that these increased attenuation values were not affected by methacholine and salbutamol challenges supports the hypothesis that bronchoconstriction played only a small or no role in attenuation changes, and that distal inflammation was a more likely contender. The ability to follow-up bronchial reactivity and lung attenuation by CT over time in cohorts of patients receiving different treatments can provide an independent tool to assess and monitor current and new therapy in asthmatic patients.

Airway wall remodeling

Asthma is known to induce structural changes in the airways including subepithelial fibrosis, mucous gland and goblet cell hyperplasia, and smooth muscle hypertrophy and hyperplasia. The latter change defines airway wall remodeling which is responsible for the faster and higher decrease related to age of forced expiratory volume per second (FEV1) in asthmatics than in controls [105]. Bronchial wall thickness measured at CT has proven to be prominent in patients with more severe asthma. This correlated with the duration and severity of the disease and the degree of air-flow obstruction [106]. This observation supports the concept that quantitative assessment of bronchial wall area at CT could be used to assess airway wall remodeling in asthmatic patients for longitudinal studies to evaluate the effects of new therapies. Such longitudinal prospective studies are needed to be carried out to monitor changes in airway wall remodeling and potential reversibility.

References

1. Ferretti GR, Bricault I, Coulomb M (2001) Virtual tools for imaging of the thorax. Eur Respir J 18:381–392
2. Hopper KD, Iyriboz TA, Mahraj RPM, Wise SW, Kasales CJ, TenHave TR, Wilson RP, Weaver JS (1998) CT bronchoscopy: optimization of imaging parameters. Radiology 209:872–877
3. Shaeffer-Prokop C, Prokop M (1996) Spiral CT of the trachea and main bronchi. In: Rémy-Jardin M, Rémy J (eds) Medical radiology spiral CT of the chest. Springer, Berlin Heidelberg New York, pp 161–183
4. Summers RM, Shaw DJ, Shelhamer JH (1998) CT virtual bronchoscopy of simulated endobronchial lesions: effect of scanning, reconstruction, and display settings and potential pitfalls. Am J Roentgenol 170:947–950
5. Rubin GD (1996) Techniques of reconstruction. In: Rémy-Jardin M, Rémy J (eds) Medical radiology spiral CT of the chest. Springer, Berlin Heidelberg New York, pp 101–127
6. Quint LE, Whyte RI, Kazerooni EA, Martinez FJ, Cascade PN, Lynch JP, Orringer MB, Brunsting LA, Deeb GM (1995) Stenosis of the central airways: evaluation by using helical CT with multiplanar reconstructions. Radiology 194:871–877
7. Rémy J, Rémy-Jardin M, Artaud D, Fribourg M (1998) Multiplanar and three-dimensional reconstruction techniques in CT: impact on chest diseases. Eur Radiol 8:335–351
8. Rémy-Jardin M, Rémy J, Deschildre F, Artaud D. Ramon P, Edme JL (1996) Obstructive lesions of the central airways: evaluation by using spiral CT with multiplanar and three-dimensional reformations. Eur Radiol 6:807–816
9. Kauczor HU, Wolcke B, Fischer B, Mildenberger P, Lorenz J, Thelen M (1996) Three-dimensional helical CT of the tracheobronchial tree: evaluation of imaging protocols and assessment of suspected stenoses with bronchoscopic correlation. Am J Roentgenol 167:419–424
10. Rémy-Jardin M, Rémy J, Artaud D, Fribourg M, Naili A (1998) Tracheobronchial tree: assessment with volume rendering – technical aspects. Radiology 208:393–398
11. Rémy-Jardin M, Rémy J, Artaud D, Fribourg M, Duhamel A (1998) Volume rendering of the tracheobronchial tree: clinical evaluation of bronchographic images. Radiology 208:761–770
12. Fetita CI, Preteux F, Beigelman-Aubry C, Grenier PA (2002) 3D Bronchoview: A new software package for investigating airway diseases. Eur Radiol 12 (Suppl 1):394
13. McAdams HP, Palmer SM, Erasmus JJ, Patz EF, Connolly JE, Goodman PC, Delong DM, Tapson VF (1998) Bronchial anastomotic complications in lung transplant recipients: virtual bronchoscopy for noninvasive assessment. Radiology 209:689–695
14. McAdams HP, Goodman PC, Kussin P (1998) Virtual bronchoscopy for directing transbronchial needle aspiration of hilar and mediastinal lymph nodes: a pilot study. Am J Roentgenol 170:1361–1364
15. McNamara AE, Muller NL, Okazawa M, Arntorp J, Wiggs BR, Pare PD (1992) Airway narrowing in excised canine lungs measured by high-resolution computed tomography. J Appl Physiol 73:307–316
16. Webb WR, Gamsu G, Wall SD, Cann CE, Proctor E (1984) CT of a bronchial phantom: factors affecting appearance and size measurements. Invest Radiol 19:394–398
17. Amirav I, Kramer SS, Grunstein M, Hoffman EA (1993) Assessment of methacholine-induced airway constriction with ultrafast high-resolution computed tomography. J Appl Physiol 75:2239–2250
18. Prêteux F, Fetita CI, Capderou A, Grenier P (1999) Modeling, segmentation, and caliber estimation of bronchi in high resolution computerized tomography. J Electron Imaging 8:36–45
19. Wood SA, Zerhouni EA, Hoford JD, Hoffman EA, Mitzner W (1995) Measurement of three-dimensional lung tree structures by using computed tomography. J Appl Physiol 79:1687–1697
20. King GG, Muller NL, Whittall KP, Xiang QS, Pare PD (2000). An analysis algorithm for measuring airway lumen and wall areas from high-resolution computed tomographic data. Am J Respir Crit Care Med 161:574–580
21. Perot V, Desberat P, Berger P, Begueret H, Elias J, Laurent F (2001) Nouvel algorithme d'extraction des paramètres géométriques des bronches en TDMHR [abstract]. J Radiol 82:1213
22. Brown R, Georakopoulos I, Mitzner W (1998) Individual canine airways responsiveness to aerosol histamine and methacholine in vivo. Am J Respir Crit Care Med 157:491–497
23. Brown R, Mitzner W, Bulut Y, Wagner E (1997) Effect of lung inflation in vivo on airways with smooth-muscle tone or edema. J Appl Physiol 82:491–499
24. Beigelman-Aubry C, Capderou A, Grenier PA, Straus C, Becquemin MH, Similowski T, Zelter M (in press) CT assessment of bronchial cross-section area and lung attenuation at controlled lung volume, in mild intermittent asthma. Radiology
25. King GG, Muller NL, Pare PD (1999) Evaluation of airways in obstructive pulmonary disease using high-resolution computed tomography. Am J Respir Crit Care Med 159:992–1004
26. Arakawa H, Webb WR, McCowin M, Katsou G, Lee KN, Seitz RF (1998) Inhomogeneous lung attenuation at thin-section CT: diagnostic value of expiratory scans. Radiology 206:89–94
27. Lee KW, Chung SY, Yang I, Lee Y, Ko EY, Park MJ (2000) Correlation of aging and smoking with air trapping at thin-section CT of the lung in asymptomatic subjects. Radiology 214:831–836
28. Verschakelen J, Scheinbaum K, Bogaert J, Demedts M, Lacquet LL, Baert AL (1998) Expiratory CT in cigarette smokers: correlation between areas of decreased lung attenuation, pulmonary function tests and smoking history. Eur Radiol 8:1391–1399
29. Bartz RR, Stern EJ (2000) Airways obstruction in patients with sarcoidosis. Expiratory CT scan findings. J Thorac Imaging 15:285–289
30. Gleeson FV, Traill ZC, Hansell DM (1996) Evidence on expiratory CT scans of small airway obstruction in sarcoidosis. Am J Roentgenol 166:1052–1054
31. Stern EJ, Frank MS (1994) Small airway diseases of the lungs: findings at expiratory CT. Am J Roentgenol 163:37–41
32. Stern EJ, Graham CM, Webb WR, Gamsu G (1993) Normal trachea during forced expiration: dynamic CT measurements. Radiology 187:27–31
33. Johnson JL, Kramer SS, Mahboubi S (1998) Air trapping in children: evaluation with dynamic lung densitometry with spiral CT. Radiology 206:95–101
34. Lucidarme O, Grenier PA, Cadi M, Mourey-Gerosa I, Benali K, Cluzel P (2000) Evaluation of air trapping at CT: comparison of continuous-versus suspended expiration CT techniques. Radiology 216:768–772
35. Gotway MB, Lee ES, Reddy GP, Golden JE, Webb WR (2000) Low-dose, dynamic, expiratory thin-section CT of the lungs using a spiral CT scanner. J Thorac Imaging 15:168–172

36. Franquet T, Stern EJ, Gimenez A, Sabaté JM, Domingo P (2000) Lateral decubitus CT: a useful adjunct to standard inspiratory–expiratory CT for the detection of air trapping. Am J Roentgenol 174:528–530
37. Fotheringham T, Chabat F, Hansell DM, Wells AU, Desai SR, Gückel C, Padley SPG, Gibson M, Yang GZ (1999) A comparison of methods for enhancing the detection of areas of decreased attenuation on CT caused by airways disease. J Comput Assist Tomogr 23:385–389
38. Ng CS, Desai SR, Rubens MB, Padley SPG, Wells AU, Hansell DM (1999) Visual quantitation and observer variation of signs of small airways disease at inspiratory and expiratory CT. J Thorac Imaging 14:279–285
39. Newman KB, Lynch DA, Newman LS, Ellegood D, Newell JD Jr (1994) Quantitative computed tomography detects air trapping due to asthma. Chest 106:105–109
40. Kalender WA, Rienmuller R, Seissler W, Behr J, Welke M, Fichte H (1990) Measurement of pulmonary parenchymal attenuation: use of spirometric gating with quantitative CT. Radiology 175:265–268
41. Millar AB, Boothroyd AE, Edwards D, Hetzel MR (1992) The role of computed tomography in the investigation of unexplained haemoptysis. Respir Med 86:39–44
42. Set PAK, Flower CDR, Smith IE, Cahn AP, Twentyman OP, Shneerson JM (1993) Hemoptysis: comparative study of the role of CT and fiberoptic bronchoscopy. Radiology 189:677–680
43. Naidich DP, Harkin TJ (1995) Airways and lung: correlation of CT with fiberoptic bronchoscopy. Radiology 197:1–12
44. McGuiness G, Beacher JR, Harkin TJ, Garay SM, Rom WN, Naidich DP (1994) Hemoptysis: prospective high-resolution CT/bronchoscopic correlation. Chest 105:1155–1162
45. Grenier P, Beigelman C (1996) Spiral CT of the bronchial tree. In: Rémy-Jardin M, Rémy J (eds) Medical radiology spiral CT of the chest. Springer, Berlin Heidelberg New York
46. Ahn JM, Im JG, Seo JW, Han HS, Yoon HK, Kim WS (1994) Endobronchial hamartoma: CT findings in three patients. Am J Roentgenol 163:49–50
47. Conces DJ, Tarver RD, Vix VA (1991) Broncholithiasis: CT features in 15 patients. Am J Roentgenol 157:249–254
48. Davis SD, Berkmen YM, King T (1989) Peripheral bronchial involvement in relapsing polychondritis: demonstration by thin-section CT. Am J Roentgenol 153:953–954
49. Im JG, Chung JW, Han SK, Han MC, Kim CW (1988) CT manifestations of tracheobronchial involvement in relapsing polychondritis. J Comput Assist Tomogr 12:792–793
50. Gaeta M, Barone M, Russi EG, Volta S, Casablanca G, Romeo P, La Spada F, Minutoli A (1993) Carcinomatous solitary pulmonary nodules: evaluation of the tumor-bronchi relationship with thin-section CT. Radiology 187:535–539
51. Westcott JL, Volpe JP (1995) Peripheral bronchopleural fistula: CT evaluation in 20 patients with pneumonia, empyema, or postoperative air leak. Radiology 196:175–181
52. Im JG, Lee WJ, Han MC, Chi JG, Han JK, Kim CW (1991) Congenital broncho-oesophageal fistula in the adult. Clin Radiol 43:380–384
53. Semenkovich JW, Glazer HS, Anderson DC, Arcidi JM Jr, Cooper JD, Patterson GA (1995) Bronchial dehiscence in lung transplantation: CT evaluation. Radiology 194:205–208
54. Schlueter FJ, Semenkovich JW, Glazer HS, Arcidi JM Jr, Trulock EP, Patterson GA (1996) Bronchial dehiscence after lung transplantation: correlation of CT findings with clinical outcome. Radiology 1999:849–854
55. Beigelman C, Howarth NR, Chartrand-Lefebvre C, Grenier P (1998) Congenital anomalies of tracheobronchial branching patterns: spiral CT aspects in adults. Eur Radiol 8:79–85
56. McGuinness G, Naidich DP, Garay SM, Davis AL, Boyd AD, Mizrachi HH (1993) Accessory cardiac bronchus: CT features and clinical significance. Radiology 189:563–566
57. Rémy-Jardin M, Rémy J, Ribet M, Gosselin B (1989) Bronchial atresia: diagnostic criteria and embryologic considerations. Diagn Intervent Radiol 1:45–51
58. Kim JS, Muller NL, Park CS, Grenier PA, Herold CJ (1997) Cylindrical bronchiectasis: diagnostic findings on thin-section CT. Am J Roentgenol 168:751–754
59. McGuinness G, Naidich DP, Leitman BS, McCauley DI (1993) Bronchiectasis: CT evaluation. Am J Roentgenol 160:253–259
60. Reiff DB, Wells AU, Carr DH, Cole PJ, Hansell DM (1995) CT findings in bronchiectasis: limited value in distinguishing between idiopathic and specific types. Am J Roentgenol 165:261–267
61. Cartier Y, Kavanagh PV, Johkoh T, Johkoh T, Mason AC, Muller NL (1999) Bronchiectasis: accuracy of high-resolution CT in the differentiation of specific diseases. Am J Roentgenol 173:47–52
62. Grenier P, Maurice F, Musset D, Menu Y, Nahum H (1986) Bronchiectasis: assessment by thin section CT. Radiology 161:95–99
63. Grenier P, Cordeau MP, Beigelman C (1993) High-resolution computed tomography of the airways. J Thorac Imaging 8:213–229
64. Kang EY, Miller RR, Muller NL (1995) Bronchiectasis: comparison of preoperative thin-section CT and pathologic findings in resected specimens. Radiology 195:649–654
65. Schoepf UJ, Becker CR, Bruening RD, Helmberger T, Staebler A, Leimeister P, Reiser MF (1999) Electrocardiographically gated thin-section CT of the lung. Radiology 212:649–654
66. Lucidarme O, Grenier PA, Coche E, Lenoir S, Aubert B, Beigelman C (1996) Bronchiectasis: comparative assessment with thin-section CT and helical CT. Radiology 200:673–679
67. Muller NL, Miller RR (1995) Diseases of the bronchioles: CT and histopathologic findings. Radiology 196:3–12
68. Akira M, Higashihara T, Sakatani M, Hara H (1993) Diffuse panbronchiolitis: follow-up CT examination. Radiology 189:559–562
69. Howling SJ, Hansell DM, Wells AU, Nicholson AG, Flint JD, Müller NL (1999) Follicular bronchiolitis: thin-section CT and histologic findings. Radiology 212:637–642
70. Matsuse T, Oka T, Kida K, Fukuchi Y (1996) Importance of diffuse aspiration bronchiolitis caused by chronic occult aspiration in the elderly. Chest 110:1289–1293
71. Matsuse T, Teramoto S, Matsui H, Ouchi Y, Fukuchi Y (1998) Widespread occurrence of diffuse aspiration bronchiolitis in patients with dysphagia, irrespective of age. Chest 114:350–351
72. Aquino SL, Gamsu G, Webb WR, Kee ST (1996) Tree-in-bud pattern: frequency and significance on thin section CT. J Comput Assist Tomogr 20:594–599
73. Gruden JF, Webb WR, Naidich DP, McGuinness G (1999) Multinodular disease: anatomic localization at thin-section CT: multireader evaluation of a simple algorithm. Radiology 210:711–720
74. Hansell DM, Moskovic E (1991) High-resolution computed tomography in extrinsic allergic alveolitis. Clin Radiol 43:8–12

75. Heyneman LE, Ward S, Lynch DA, Rémy-Jardin M, Johkoh T, Muller NL (1999) Respiratory bronchiolitis, respiratory bronchiolitis-associated interstitial lung disease, and desquamative interstitial pneumonia: different entities of part of the spectrum of the same disease process? Am J Roentgenol 173:1617–1622
76. Lynch DA (2001) High-resolution CT of idiopathic interstitial pneumonias. Radiol Clin North Am 39:1153–1170
77. Muller NL, Staples CA, Miller RR (1990) Bronchiolitis obliterans organizing pneumonia: CT features in 14 patients. Am J Roentgenol 154:983–987
78. Lee KS, Kullnig P, Hartman TE, Muller NL (1994) Cryptogenic organizing pneumonia: CT findings in 43 patients. Am J Roentgenol 162:543–546
79. Akira M, Yamamoto S, Sakatani M (1998) Bronchiolitis obliterans organizing pneumonia manifesting as multiple large nodules or masses. Am J Roentgenol 107:291–295
80. Worthy SA, Park CS, Kim JS, Muller NL (1997) Bronchiolitis obliterans after lung transplantation: high-resolution CT findings in 15 patients. Am J Roentgenol 169:673–677
81. Yang CF, Wu MT, Chiang AA, Lai RS, Chen C, Tiao WM, McLoud TC, Wang JS, Pan HB (1997) Correlation of high-resolution CT and pulmonary function in bronchiolitis: a study based on 24 patients associated with consumption of Sauropus Androgynus. Am J Roentgenol 168:1045–1050
82. Miller RR, Muller NL (1995) Neuroendocrine cell hyperplasia and obliterative bronchiolitis in patients with peripheral carcinoid tumors. Am J Surg Pathol 19:653–658
83. Worthy SA, Muller NL, Hartman TE, Swensen SJ, Padley SPG, Hansell DM (1997) Mosaic attenuation pattern on thin-section CT scans of the lung: differentiation among infiltrative lung, airway, and vascular diseases as a cause. Radiology 205:465–470
84. Moore AD, Godwin JD, Dietrich PA, Verschakelen JA, Henderson WR Jr (1992) Swyer-James syndrome: CT findings in eight patients. Am J Roentgenol 158:1211–1215
85. Leung AN, Fisher K, Valentine V, Girgis RE, Berry GJ, Robbins RC, Theodore J (1998) Bronchiolitis obliterans after lung transplantation: detection using expiratory HRCT. Chest 113:365–370
86. Hansell DM, Wells AU, Padley SP, Muller NL (1996) Hypersensitivity pneumonitis: correlation of individual CT patterns with functional abnormalities. Radiology 199:123–128
87. Hansell DM, Rubens MB, Padley SP, Wells AU (1997) Obliterative bronchiolitis: individual CT signs of small airway disease and functional correlation. Radiology 203:721–726
88. Lucidarme O, Coche E, Cluzel P, Mourey-Gerosa I, Howarth N, Grenier P (1998) Expiratory CT scans for chronic airway disease: correlation with pulmonary function test results. Am J Roentgenol 170:301–307
89. Padley SPG, Adler BD, Hansell DM, Muller NL (1993) Bronchiolitis obliterans: high-resolution CT findings and correlation with pulmonary function tests. Clin Radiol 47:236–240
90. Roberts HR, Wells AU, Milne DG, Rubens MB, Kolbe J, Cole PJ, Hansell DM (2000) Airflow obstruction in bronchiectasis: correlation between computed tomography features and pulmonary function tests. Thorax 55:198–204
91. Tagasuki JE, Godwin D (1998) Radiology of chronic obstructive pulmonary disease. Radiol Clin North Am 36:39–55
92. Stark P, Norbash A (1998) Imaging of the trachea and upper airways in patients with chronic obstructive airway disease. Radiol Clin North Am 36:91–105
93. Gilkeson RC, Ciancibello LM, Hejal RB, Montenegro HD, Lange P (2001) Tracheobronchomalacia: dynamic airway evaluation with multidetector CT. Am J Roentgenol 176:205–210
94. Remy-Jardin M, Remy J, Boulenguez C, Sobaszek A, Edme JL, Furon D (1993) Morphologic effects of cigarette smoking on airways and pulmonary parenchyma in healthy adult volunteers: CT evaluation and correlation with pulmonary function tests. Radiology 186:107–115
95. Remy-Jardin M, Edme JL, Boulenguez C, Remy J, Mastora L, Sabaszek A (2002) Longitudinal follow-up study of smoker's lung with thin section CT in correlation with pulmonary function tests. Radiology 222:261–270
96. Lamers RJ, Thelissen GR, Kessels AG, Wouters EF, van Engelshoven JM (1994) Chronic obstructive pulmonary disease: evaluation with spirometrically controlled CT lung densitometry. Radiology 193:109–113
97. Gevenois PA, de Vuyst P, Sy H, Scillia P, Chaminade L, de Maertelaer V, Zanen J, Yernault JC (1996) Pulmonary emphysema: quantitative CT during expiration. Radiology 199:825–829
98. Gevenois PA, de Maertelaer V, de Vuyst P, Zanen J, Yernault JC (1995) Comparison of computed density and macroscopic morphometry in pulmonary emphysema. Am J Respir Crit Care Med 152:653–657
99. Lynch DA (1998) Imaging of asthma and allergic bronchopulmonary mycosis. Radiol Clin North Am 36:129–142
100. Grenier P, Mourey-Gerosa I, Benali K, Brauner MW, Leung AN, Lenoir S, Cordeau MP, Mazoyer B (1996) Abnormalities of the airways and lung parenchyma in asthmatics: CT observations in 50 patients and inter- and intraobserver variability. Eur Radiol 6:199–206
101. Lynch DA, Newell JD, Tschomper BA, Cink TM, Newman LS, Bethel R (1993) Uncomplicated asthma in adults: comparison of CT appearance of the lungs in asthmatic and healthy subjects. Radiology 188:829–833
102. Paganin F, Trussard V, Seneterre E, Chanel P, Giron J, Godard P, Senac JP, Michel B, Bousquet J (1992) Chest radiography and high resolution computed tomography of the lungs in asthma. Am Rev Respir Dis 146:1084–1087
103. Park CS, Muller NL, Worthy SA, Kim JS, Awadh N, Fitzgerald M (1997) Airway obstruction in asthmatic and healthy individuals: inspiratory and expiratory thin-section CT findings. Radiology 203:361–367
104. Wollmer P, Albrechtsson U, Brauer K, Eriksson L, Johnson B, Tylen B (1986) Measurement of pulmonary density by means of X-ray computerized tomography. Relation to pulmonary mechanics in normal subjects. Chest 90:387–391
105. Lange P, Parner J, Vestbo J, Schnohr P, Jensen G (1998) A 15-year follow-up study of ventilatory function in adults with asthma. N Engl J Med 339:1194–2000
106. Nimi A, Matsumoto H, Amitani R, Nakano Y, Mishima M, Minakuchi M, Nishimura K, Itoh H, Izumi T (2000) Airway wall thickness in asthma assessed by computed tomography. Relation to clinical indices. Am J Respir Crit Care Med 162:1518–1523